

Sub-Band Spectral Matching with Localized Score Aggregation for Robust Anomalous Sound Detection

Phurich Saengthong¹, Takahiro Shinozaki¹

Abstract—Detecting subtle deviations in noisy acoustic environments is central to anomalous sound detection (ASD). A common training-free ASD pipeline temporally pools frame-level representations into a band-preserving feature vector and scores anomalies using a single nearest-neighbor match. However, this global matching can inflate normal-score variance through two effects. First, when normal sounds exhibit band-wise variability, a single global neighbor forces all bands to share the same reference, increasing band-level mismatch. Second, cosine-based matching is energy-coupled, allowing a few high-energy bands to dominate score computation under normal energy fluctuations and further increase variance. We propose BEAM, which stores temporally pooled sub-band vectors in a memory bank, retrieves neighbors per sub-band, and uniformly aggregates scores to reduce normal-score variability and improve discriminability. We further introduce a parameter-free adaptive fusion to better handle diverse temporal dynamics in sub-band responses. Experiments on multiple DCASE Task 2 benchmarks show strong performance without task-specific training, robustness to noise and domain shifts, and complementary gains when combined with encoder fine-tuning.

Index Terms—anomaly detection, anomalous sound detection, domain generalization

I. INTRODUCTION

ANOMALIES are defined not only by what they are, but by how they deviate from expectations. In acoustics, even subtle sound variations can reveal hidden faults that would otherwise go unnoticed. This motivates anomalous sound detection (ASD) for industrial condition monitoring, where an ASD system assigns an anomaly score to each clip and raises an alarm when the score crosses a threshold [1]–[5]. Because abnormal events are rare and diverse, ASD is typically trained in a semi-supervised setting using only normal data [6], [7]. In deployment, shifts in background noise, environment, or operating conditions can widen the normal-score distribution and destabilize fixed thresholds. For example, a normal machine recording can exceed a threshold tuned on training data when the noise floor rises, causing false alarms and frequent retuning.

Recent state-of-the-art (SOTA) ASD systems [8]–[13] adopt a *global matching* design, where each clip is summarized by a single clip-level embedding and compared to a reference memory via nearest-neighbor (NN) search, most commonly using cosine similarity. In this framework, domain shift from changing machine operating conditions or noise, and the resulting threshold instability, is often addressed with score normalization or calibration [9], [10], [12], [13]. GenRep-style

systems [9], [10], [13] show that large-scale, general-domain pre-trained audio encoders can deliver strong performance and robustness under domain shift, while remaining competitive with target-machine encoder fine-tuning [10], [14]. This makes global matching a compact, practical *training-free* baseline when task-specific training is infeasible, requiring only storage of reference embeddings for rapid deployment across diverse machine operating and recording conditions with minimal target-machine tuning.

In signal detection theory (SDT), detection degrades when the normal-score distribution broadens relative to normal–anomalous separation. We analyze a failure mode of global cosine matching that increases normal-score variance through two mechanisms. Consider normal machine sounds whose underlying state is unchanged, but whose test recordings have low SNR and background-noise conditions different from those represented in the references stored in the memory bank. Let the clip embedding be decomposed into sub-bands (i.e., fixed feature partitions), and suppose that normal recording-condition variation perturbs these sub-bands unequally. Global cosine matching then selects a single nearest-neighbor reference using the full clip embedding consisting of these sub-bands. Because cosine similarity in this setting is magnitude-coupled, higher-magnitude sub-bands contribute more to both reference selection and final score computation. This leads to two variance-inflating effects: first, the best whole-embedding neighbor need not be the best match for each sub-band, so reusing it across sub-bands creates residual mismatches that widen the normal-score distribution. Second, a few high-magnitude sub-bands can disproportionately influence the final score, causing variation in those sub-bands to contribute more to normal-score variation. Consequently, anomaly decisions become less reliable even when the underlying machine state remains normal.

Motivated by these two effects, we propose *BEAM* (Band-wise Equalized Anomaly Measure), a simple k -NN-based scoring method that replaces single-reference global matching with band-aligned sub-band matching and uniform aggregation. Given a clip-level *frequency-derived* representation, *BEAM* stores reference descriptors in a band-aligned memory bank of sub-band embeddings shared across reference domains; at inference, each sub-band queries its corresponding bank and the band scores are aggregated uniformly. This per-band retrieval can decouple reference selection across sub-bands, reducing tied-reference mismatch, while uniform aggregation can remove energy coupling and prevent high-magnitude sub-bands from dominating the final score, thereby stabilizing normal scores. We further introduce *AdaBEAM*, which integrates Dynamic Mean–Max (DMM) scoring by

¹ Department of Information and Communications Engineering, Institute of Science Tokyo, Japan (e-mail: saengthong.p.aa@m.titech.ac.jp; website: <http://www.ts.ip.titech.ac.jp>).

Manuscript under review.

maintaining temporally mean-pooled and max-pooled sub-band memories, scoring both views, and fusing clip-level scores with a simple parameter-free rule. Finally, we formalize how sub-band matching and uniform aggregation can reduce normal-score variance and provide an SDT-based sufficient condition showing when this variance gain outweighs any accompanying change in mean separation.

We evaluate *BEAM* across several feature families, including both handcrafted and pre-trained clip representations. For spectrogram-derived features, we use temporally pooled log-Mel, MFCC, and deep spectrogram embeddings from pre-trained audio encoders. We also include LPC spectra, which, although explored in prior ASD work, remain relatively underused compared with spectrogram-derived features. Their ability to capture both smooth spectral envelopes and narrow-band resonances makes them a natural match for our focus on fine-grained spectral structure. On DCASE Task 2 benchmarks [5], [15], [16] under the standard evaluation protocols, *BEAM* and its adaptive variant *AdaBEAM* achieve strong performance among training-free systems in Official Score when combined with frozen, pre-trained audio encoders. Moreover, *BEAM* remains effective with handcrafted features, surpassing task-specific trained autoencoder baselines. In this spectrogram-derived instantiation, *AdaBEAM* further improves detection performance over *BEAM* in both noisy and domain-shift settings by fusing complementary temporally mean-pooled and max-pooled views via DMM. Beyond the training-free setting, *BEAM/AdaBEAM* also yield consistent improvements over the corresponding global-matching baselines when the encoder is fine-tuned with task-specific objectives on target-machine data, although our primary focus is on the training-free regime.

We make the following contributions:

- **Variance-focused analysis of global matching:** we characterize how tied-reference retrieval and energy-coupled aggregation contribute to normal-score variance inflation under domain shift and noise.
- **BEAM scoring:** we introduce *BEAM*, which performs band-aligned sub-band retrieval with uniform aggregation, and describe its variant *AdaBEAM*, which fuses mean- and max-pooled views via Dynamic Mean-Max (DMM) scoring.
- **SDT-based condition for improved sensitivity:** we derive a sufficient condition under which variance reduction yields a net gain in detection sensitivity d' relative to global cosine matching.
- **Empirical validation on DCASE Task 2:** the proposed methods achieved strong training-free performance across different feature types, remained competitive with several methods that rely on task-specific training, and further provided consistent gains in fine-tuned settings under noise and domain shift.

II. PRELIMINARY: GLOBAL BAND MATCHING

This section formalizes the tied-reference global-matching formulation that *BEAM* builds on. Each audio clip is mapped to a clip-level representation, and anomaly evidence is computed from a single nearest-neighbor match in that representation space [9], [12], [13], [17]. We first define the clip

representations used in this work, then summarize the standard global-matching (k -NN) score used in recent systems (e.g., GenRep-style pipelines [9], [13]), and finally analyze the structure and limitations of exact global cosine scoring.

A. Clip-Level Representations

We represent each audio clip by a vector $f \in \mathbb{R}^F$ whose coordinates follow an ordered feature axis (e.g., frequency bins, spectral bands, or ordered spectral-derived coefficients). We assume this axis can be partitioned into meaningful sub-bands. In this work, we instantiate f using three front-end families: (i) handcrafted frame-level spectral/cepstral features followed by temporal pooling (Log-Mel filterbank energies and MFCCs), (ii) spectrogram-based embeddings from large-scale pretrained encoders that produce patch-level features before pooling, and (iii) LPC spectra, obtained directly from all-pole signal modeling rather than from frame-level temporal pooling.

1) *Temporally pooled spectral and cepstral features:* Let $X \in \mathbb{R}^{T \times F}$ denote a frame-level feature matrix, where T is the number of frames and F is the feature dimension. For spectral features such as Log-Mel filterbank energies [17], index j corresponds to a mel-frequency band. For cepstral features such as MFCCs, index j corresponds to an ordered cepstral coefficient. Although the MFCC axis is not a frequency-band axis, it is ordered and can be partitioned; therefore, we include MFCCs as an additional instantiation of f .

Clip-level features are obtained by pooling X over time:

$$f(j) = \begin{cases} \frac{1}{T} \sum_{t=1}^T X(t, j), & \text{(temporal mean pooling),} \\ \max_t X(t, j), & \text{(temporal max pooling),} \end{cases} \quad (1)$$

for $j = 1, \dots, F$. The resulting vector $f \in \mathbb{R}^F$ summarizes the entire recording over time while preserving an ordered feature axis (frequency for Log-Mel, coefficient index for MFCCs).

2) *Spectrogram embeddings from pretrained encoders:* For Transformer-based encoders [18] such as BEATs [19], the input spectrogram is divided into a grid of time-frequency patches, each mapped to a D -dimensional embedding. This yields patch embeddings $h \in \mathbb{R}^{L \times D}$ with $L = T_p \cdot F_p$, where T_p and F_p are the numbers of patch positions along time and frequency, respectively. We reshape h into $T_p \times F_p \times D$, group embeddings by frequency index, and apply temporal pooling over the T_p patches within each frequency band to obtain F_p band descriptors in \mathbb{R}^D . Concatenating these per-band embeddings yields a clip-level representation $f \in \mathbb{R}^{F_p \cdot D}$ whose coordinates remain organized by frequency band. Encoders fine-tuned on reference-machine data using auxiliary objectives [8], [20], [21] can be used in the same way.

3) *LPC spectrum:* LPC spectra form a complementary handcrafted feature class. Unlike spectrogram-derived features, which are computed per frame and then temporally pooled, LPC spectra are obtained by fitting an all-pole model directly to the waveform and sampling its magnitude response. Compared with FFT-based spectra, the all-pole model yields a smoother envelope that can make resonant peaks more salient and easier to localize.

Given a waveform segment $s(n)$, we estimate LPC coefficients $\{a_k\}_{k=1}^p$ (e.g., via Burg's method [22], [23]). Sampling the magnitude response of the resulting all-pole model at F frequency bins yields an LPC spectrum feature $f \in \mathbb{R}^F$:

$$f[m] \triangleq \left| \frac{1}{1 - \sum_{k=1}^p a_k e^{-j\omega_m k}} \right|, \quad m = 1, \dots, F. \quad (2)$$

B. Tied-Reference Global Matching

GenRep-style training-free ASD systems [9], [10], [13] typically score a test clip by global nearest-neighbor matching against a normal reference memory, optionally followed by score normalization (e.g., domain-wise normalization [9], [10] or local density normalization [12], [13]). Here, we analyze the core tied-reference global-matching score before such normalization. Given a clip-level representation $f_y \in \mathbb{R}^F$ and a normal reference memory $\mathcal{M}_{\text{glob}} = \{f_i\}_{i=1}^R$ (with R normal reference clips), the global-matching pipeline scores test clip y using its single nearest neighbor under cosine similarity:

$$i^*(y) = \arg \max_{i \in \{1, \dots, R\}} \langle \hat{f}_y, \hat{f}_i \rangle, \quad (3)$$

$$S_{\text{glob}}(y) \triangleq d_{\text{NN}}(f_y, \mathcal{M}_{\text{glob}}) = \frac{1}{2} \left(1 - \langle \hat{f}_y, \hat{f}_{i^*(y)} \rangle \right),$$

where $\hat{x} \triangleq x / \|x\|_2$ denotes ℓ_2 -normalization.

1) *Global Band Cosine Decomposition*: To analyze how this tied-reference score behaves across frequency, we decompose $S_{\text{glob}}(y)$ into sub-band contributions. We partition the feature axis into N_b disjoint sub-bands. Let $w_{y,j}$ and $w_{i^*(y),j}$ denote the sub-band- j slices of test clip y and its global nearest neighbor $i^*(y)$, and let $s_j(y) \triangleq \langle \hat{w}_{y,j}, \hat{w}_{i^*(y),j} \rangle$ denote the local sub-band similarity. Define the sub-band energy weights as $\beta_j(y) \triangleq \|w_{y,j}\| \|w_{i^*(y),j}\| / (\|f_y\| \|f_{i^*(y)}\|)$ and the total energy coupling as $\rho(y) \triangleq \sum_{j=1}^{N_b} \beta_j(y)$. Then the global score decomposes exactly as

$$S_{\text{glob}}(y) = \frac{1}{2} \left(1 - \rho(y) \sum_{j=1}^{N_b} \tilde{\beta}_j(y) s_j(y) \right), \quad (4)$$

where $\tilde{\beta}_j(y) \triangleq \beta_j(y) / \rho(y)$ are normalized weights.

This decomposition makes two limitations of tied-reference global matching explicit, both of which can be amplified by domain shift or added noise: (i) all bands share the same nearest-neighbor index $i^*(y)$, so $s_j(y)$ reflects a global compromise rather than a band-wise best match; and (ii) the aggregation is energy-coupled through the data-dependent weights $\beta_j(y)$, which can shift with recording conditions and concentrate mass on a few bands. Both effects can increase normal-score variability and motivate variance-reduced alternatives. See Appendix for full definitions and derivation.

III. METHOD

We propose *BEAM* to mitigate the variance inflation of tied-reference global matching (Sec. II-B) through band-aligned retrieval and uniform aggregation. Sec. III-A defines a band-aligned memory bank of sub-band descriptors, and Sec. III-B introduces band-restricted nearest-neighbor scoring with uniform aggregation. To capture both stable and transient

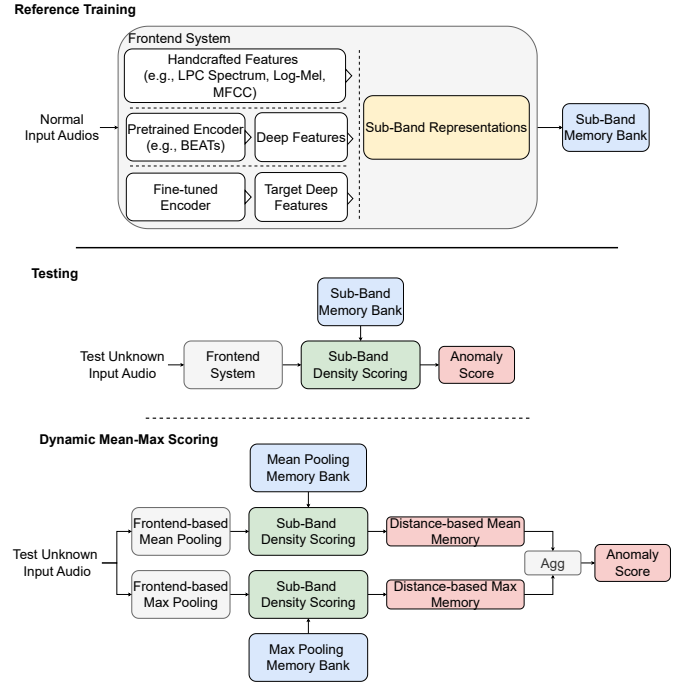


Fig. 1. Overview of *BEAM* and *AdaBEAM*. Normal audio is mapped to handcrafted or deep features, sliced into sub-bands, and stored in a shared memory bank. At test time, each query sub-band is matched within its band-aligned memory, and the resulting band scores are uniformly aggregated to produce the anomaly score. *AdaBEAM* adds Dynamic Mean-Max (DMM) fusion by building mean- and max-pooled sub-band memories, scoring both views, and combining the resulting clip scores with a simple parameter-free rule.

temporal patterns, Sec. III-C extends this design to *AdaBEAM* by fusing scores from temporal mean and temporal max pooling via Dynamic Mean-Max (DMM) integration. Fig. 1 summarizes the full pipeline.

A. Memory Bank of Sub-Band Embeddings

Given a clip representation $f \in \mathbb{R}^F$ (obtained either by temporal pooling of a time-frequency feature or directly from an LPC spectrum; Sec. II-A), we partition each reference descriptor f_i into N_b contiguous sub-bands:

$$\mathbf{w}_{i,j} = f_i[\mathcal{I}_j] \in \mathbb{R}^{\mathcal{I}_j}, \quad j = 1, \dots, N_b,$$

$$\mathcal{I}_j = \{1 + (j-1)s, \dots, 1 + (j-1)s + C - 1\},$$

where C and s are the window size and stride, yielding $N_b = 1 + \lfloor (F - C) / s \rfloor$ band positions. We maintain a band-aligned memory bank for each position,

$$\mathcal{M}_j \triangleq \{\mathbf{w}_{i,j}\}_{i=1}^R, \quad j = 1, \dots, N_b,$$

where R denotes the number of normal reference samples. We denote the full memory as $\mathcal{M} = \{\mathcal{M}_j\}_{j=1}^{N_b}$.

B. Local Matching and Clip-Level Aggregation

Given a test clip y , we form its sub-band descriptors $\{\mathbf{w}_j(y)\}_{j=1}^{N_b}$ and score each band by a band-restricted nearest-neighbor distance:

$$d_{\text{sub}}(\mathbf{w}_j(y)) = \min_{\mathbf{w} \in \mathcal{M}_j} d_{\text{NN}}(\mathbf{w}_j(y), \mathbf{w}), \quad j = 1, \dots, N_b, \quad (5)$$

where $d_{NN}(\cdot, \cdot)$ is the cosine distance defined in Sec. II-B. The clip-level score is the uniform aggregation of band-wise distances:

$$S_{\text{sub}}(y) \triangleq \frac{1}{N_b} \sum_{j=1}^{N_b} d_{\text{sub}}(\mathbf{w}_j(y)).$$

The score $S_{\text{sub}}(y)$ already defines a valid clip-level anomaly measure and directly instantiates the variance-motivated design in Sec. II-B1. In practice, however, the raw sub-band distances $\{d_{\text{sub}}(\mathbf{w}_j(y))\}$ can exhibit band- and domain-dependent scales (e.g., different local noise floors). To improve cross-band comparability before aggregation, we apply local density normalization (LDN) [12] at the sub-band level and define the normalized distance as:

$$d_{\text{sub}}^{\text{norm}}(\mathbf{w}_j(y)) \triangleq \min_{\mathbf{w} \in \mathcal{M}_j} \frac{d_{NN}(\mathbf{w}_j(y), \mathbf{w})}{\sum_{k=1}^K d_{NN}(\mathbf{w}, \mathbf{w}_k)}, \quad (6)$$

where $\{\mathbf{w}_k\}_{k=1}^K$ are the K nearest neighbors of the matching sample \mathbf{w} within the same band-aligned memory \mathcal{M}_j . The denominator estimates the local neighborhood scale around \mathbf{w} within \mathcal{M}_j , calibrating distances before aggregation. Unlike clip-level normalization, which applies a single global scale, sub-band LDN uses band-local scales so that no band systematically dominates the uniform aggregation. The resulting clip-level score is the uniform aggregation of normalized band scores:

$$S_{\text{sub}}^{\text{norm}}(y) \triangleq \frac{1}{N_b} \sum_{j=1}^{N_b} d_{\text{sub}}^{\text{norm}}(\mathbf{w}_j(y)). \quad (7)$$

C. Dynamic Mean–Max Integration (DMM)

To handle diverse temporal dynamics, *AdaBEAM* computes two parallel clip-level scores: $S_{\text{Tmean}}(y)$ from temporal mean pooling, which captures stable spectral structure, and $S_{\text{Tmax}}(y)$ from temporal max pooling, which emphasizes transient high-energy peaks. We integrate them using a simple parameter-free rule:

$$S_{\text{DMM}}(y) = \text{agg}(S_{\text{Tmean}}(y), S_{\text{Tmax}}(y)), \quad (8)$$

where agg denotes a fusion operator. By default, we use the mean, and we evaluate alternative choices in our analysis.

Building on the variance-inflation mechanism identified for global matching in Sec. II-B1, Sec. IV provides a theoretical analysis showing how sub-band scoring can reduce normal-score variance and, from an SDT perspective, admit a sufficient condition for improved detection sensitivity (d'). Full derivations are deferred to the Appendix.

IV. THEORETICAL ANALYSIS

We analyze *BEAM* at the score level under broad normal operating-condition variability (e.g., machine-state changes and background noise). Proposition 1 upper-bounds the normal-score variance of sub-band scoring by a constant multiple of tied-reference global matching. Theorem 1 converts this variance bound into a sufficient condition for improved SDT sensitivity d' , determined by how well the anomalous–normal mean gap is preserved. For readability, we keep the

main statements in this section and defer setup details, formal definitions, and full derivations to Appendix.

The DMM fusion rule is a complementary design choice applied after computing two view-specific scores, each based on a fixed pooling operator (e.g., T_{mean} or T_{max}). Qualitatively, mean fusion can reduce normal-score variance when the two view fluctuations are not perfectly correlated, whereas max fusion preserves sharp intermittent anomalies that averaging may dilute; we validate this trade-off empirically in Sec. VII. For clarity, Proposition 1 and Theorem 1 are stated for the *raw* scores (without LDN), while LDN is treated as an orthogonal calibration layer and evaluated empirically.

Proposition 1. *Assume all random variables and their first- and second-order moments appearing in the analysis are finite and $0 < \text{Var}(S_{\text{sub}} | \mathcal{N}) < \infty$ and $0 < \text{Var}(S_{\text{glob}} | \mathcal{N}) < \infty$. Let $C_{\text{var}} \geq 0$ be the variance ratio constant defined in Appendix Eq. (11). This constant aggregates the net effect of switching (i) from tied-reference global matching to band-aligned retrieval and (ii) from energy-coupled global aggregation to uniform aggregation, with regime drift handled via the total-variance decomposition in Appendix Sec. B. Then*

$$\text{Var}(S_{\text{sub}} | \mathcal{N}) \leq C_{\text{var}} \text{Var}(S_{\text{glob}} | \mathcal{N}). \quad (9)$$

Using the variance-ratio bound C_{var} in (9), we now derive a sufficient condition for improved detection sensitivity.

Theorem 1. *Under the assumptions of Proposition 1, assume the anomalous mean score exceeds the normal mean score for global matching (i.e., $\Delta(S_{\text{glob}}) > 0$), where $\Delta(S)$ denotes the anomalous–normal mean gap. Let $d'(S)$ denote the standard signal-detection sensitivity index (defined in Appendix Sec. A). If the mean gap of sub-band scoring satisfies $\Delta(S_{\text{sub}}) \geq \sqrt{C_{\text{var}}} \Delta(S_{\text{glob}})$, then*

$$d'(S_{\text{sub}}) \geq d'(S_{\text{glob}}). \quad (10)$$

Theorem 1 shows that d' improves when mean-gap attenuation is no worse than the normal standard-deviation reduction implied by Proposition 1. Accordingly, our diagnostics report both the variance ratio and the mean-gap ratio across band sizes to verify this trade-off (see Sec. VII-A and Appendix Sec. C).

V. RELATED WORK

This work builds on ASD systems developed in the DCASE community, particularly Task 2 [5], [14]–[16], [24]–[26]. A large part of this literature improves ASD through *task-specific training*. Early approaches fit generative models to normal data and score anomalies by reconstruction error or likelihood; representative examples include [1], [27]–[40]. Later work shifted toward discriminative or OE-based objectives [41], often learning noise-robust embeddings (e.g., with machine-type metadata) and applying lightweight back-ends such as k-NN [42]. These embeddings are either trained from scratch [12], [13], [17], [20], [43]–[49] or obtained by fine-tuning pre-trained encoders [8], [11], [13], [50]–[54]. More recently, large-scale self-supervised encoders have shown competitive Task 2 performance without OE training or fine-tuning [9],

[10], [55]. In this setting, *BEAM* targets a complementary axis by improving *training-free* anomaly scoring with fixed representations.

BEAM builds on large-scale self-supervised audio encoders pre-trained on datasets such as AudioSet [19], [56]–[64], which yield transferable representations, especially when paired with temporal mean pooling [9], [13], [59]. Representative frameworks such as GenRep [9] and AnoPatch [8] combine these encoders with lightweight nearest-neighbor back-ends on clip-level embeddings: GenRep uses temporal mean-pooled BEATs [19] with MemMixup and domain-score normalization, whereas AnoPatch applies patch pooling on a BEATs model fine-tuned with machine-specific meta-information. Both score a test clip via a *tied-reference* global match against domain-specific reference banks, then select a relative score across domains. In contrast, *BEAM* preserves frequency resolution after temporal pooling and performs band-aligned nearest-neighbor matching against *domain-agnostic* memory banks shared across domains, followed by uniform aggregation across sub-bands.

BEAM can be combined with LDN approaches [10], [12], [13], which normalize anomaly scores and can support more stable thresholding under domain shift. Prior work typically applies LDN to a *single* clip-level anomaly score obtained from global matching. In contrast, we apply LDN to *sub-band* nearest-neighbor distances before uniform aggregation, calibrating band-wise distances prior to fusion. We also analyze the effect of the neighborhood size K in sub-band LDN on score calibration and robustness.

The proposed DMM scoring is related to prior methods that applied temporal pooling of spectrogram features to balance robustness and sensitivity in anomaly detection. Wilkinghoff et al. [17] showed that combining temporal pooling with GMMs yields the best results when mean or max pooling is chosen per machine type. Guan et al. [38] introduced time-weighted pooling to balance mean and max effects but still required machine-specific tuning. In contrast, DMM fuses *two BEAM scores* computed from mean- and max-pooled views, avoiding machine-specific selection while keeping the backend unchanged.

The proposed sub-band matching is conceptually related to prior sub-band modeling in audio understanding [65]–[67]. Fisher [65] extracts frequency-wise representations as transformer inputs to address variations across sampling rates, producing global embeddings for ASD. Sound event detection methods [66], [67] similarly exploit frequency-dependent modeling to capture fine-grained sub-band dependencies using convolutional or attention mechanisms. In contrast, *BEAM* is training-free: it scores temporally pooled clip descriptors via band-aligned sub-band retrieval and uniform aggregation, rather than learning frequency-dependent feature representations.

Our work also builds on LPC [22], [23], [68], [69], a classic technique for modeling spectral envelopes. Unlike [70], which uses LPC-derived features to train a VAE on short segments, we compute clip-level LPC spectra and apply k-NN scoring directly without additional training. We then evaluate this descriptor within the proposed *BEAM* framework, where it

TABLE I
PER-SECTION STATISTICS OF EACH MACHINE TYPE IN THE CONSIDERED ASD DATASETS.

Dataset (sec-dev & sec-eval)	Split	Source domain		Target domain	
		Normal	Anomalous	Normal	Anomalous
DCASE2020T2 [5]	Train	-	-	≤ 1000	-
	Test	-	-	≤ 400	≤ 200
DCASE2023T2 [15]	Train	990	-	10	-
	Test	50	50	50	50
DCASE2024T2 [16]	Train	990	-	10	-
	Test	50	50	50	50
MIMII [3] (No sec-dev or sec-eval)	Train	-	-	≤ 934	-
	Test	-	-	≤ 407	≤ 407

captures timbre-related spectral-envelope differences [71].

BEAM with pre-trained audio transformers can be viewed as a patch-level variant, conceptually related to patch-based industrial image anomaly detection (AD) [72]–[75]. Here, we form “patches” by first extracting ViT-style token embeddings [75], [76] and then collapsing the time axis to obtain frequency-indexed descriptors, so each band summarizes the entire clip over time within a frequency range. Accordingly, we aggregate scores uniformly across bands, whereas image patch AD typically applies max pooling over spatial locations to emphasize localized defects.

VI. EXPERIMENTAL DETAILS

A. Data

We use DCASE Task 2 benchmarks for the main evaluations, following [12], [13]: DCASE2020T2 [5] for single-domain performance, and DCASE2023T2 [15] plus DCASE2024T2 [16] for domain-shift robustness (Table I). We also use MIMII [3] for the clip-level feature analysis in Sec. VII-C.

MIMII. MIMII contains normal and anomalous recordings from four machine types (Fan, Pump, Slider, and Valve) captured in real factory environments at SNRs of -6, 0, and 6 dB [3]. Fan and Pump primarily produce stationary sounds, whereas Slider and Valve are more non-stationary. Each machine type has four sections, and each SNR subset contains about 18k clips under the train/test split in [77].

DCASE2020T2. The DCASE2020T2 benchmark [5] focuses on the evaluation of individual machine types, including Toy-Car and ToyConveyor from the ToyADMOS [78] dataset, and Fan, Pump, Slider, and Valve from the MIMII dataset [3]. It is divided into two sections, the DCASE2020T2 Development Set (sec-dev) and the DCASE2020T2 Evaluation Set (sec-eval). While both sections cover the same machine types, they differ in their machine sections and therefore exhibit distinct acoustic characteristics. All recordings are single-channel at 16 kHz.

DCASE2023T2 and **DCASE2024T2.** These benchmarks [15], [16], [79]–[82] evaluate domain generalization (DG) by introducing distribution shifts in the reference normal data, resembling a long-tail setting. Each benchmark has a Development Set (sec-dev) and an Evaluation Set (sec-eval). The sec-dev split includes seven machine types from [80], whereas sec-eval differs: DCASE2023T2 uses seven types

from [81], and DCASE2024T2 uses nine types from [81], [82]. Each machine type corresponds to one section with distinct attributes, although some sections in DCASE2024T2 lack explicit annotations. The sec-dev machine types are similar across benchmarks, while sec-eval machine types are disjoint. All recordings are single-channel at 16 kHz, with durations of 6–18 s (typically 10–12 s).

B. Metrics

We report performance using the area under the receiver operating characteristic (ROC) curve (AUC) and the partial AUC (pAUC) over a low false positive rate (FPR) range $[0, p]$, following [5]. The ROC curve plots the true positive rate (TPR) against the FPR as the anomaly-score threshold is varied. AUC can be interpreted as the probability that a randomly chosen anomalous sample receives a higher anomaly score than a randomly chosen normal sample. pAUC computes the same ranking-based quantity but restricts attention to the ROC segment with $FPR \leq p$, emphasizing performance under strict false-alarm constraints. We use $p = 0.1$ [5].

For MIMII and DCASE2020T2 (sec-dev and sec-eval), we follow [12] and report the arithmetic mean of AUC and pAUC, where each metric is first averaged across machine sections. For the domain-shift benchmarks (DCASE2023T2 and DCASE2024T2, sec-dev and sec-eval), we follow the Official Score definition [15], [16]: for each machine type, we compute the harmonic mean of (i) source-domain AUC, (ii) target-domain AUC, and (iii) mixed-domain pAUC. The final Official Score is the harmonic mean across machine types.

We also report the detection sensitivity index $d'(S) = \Delta(S) / \sqrt{\text{Var}(S | \mathcal{N})}$, which measures score separation between anomalous and normal samples relative to the variability of normal scores; larger d' indicates easier detection. See Appendix Sec. A for the full SDT definition.

C. Implementation Details

1) *Baseline Training-free Frontend System:* We use both handcrafted and deep spectrogram features. Log-Mel features use 128 mel bins over 0–8000 Hz with frame length 64 and frame shift 32. MFCCs use 90 coefficients with the same frequency range and frame parameters. For LPC, we extract 60 LPC coefficients using Librosa [83]; for LPC spectrum, we convert these 60 coefficients into an 8000-bin frequency response up to Nyquist. Each audio segment is zero-padded or truncated to 10 s. For deep features, we use frozen embeddings from the last Transformer layer of BEATs iter3 [19], EAT [63] (epoch 30), and EAT-large (epoch 20). The model sizes are approximately 90 M parameters (BEATs iter3), 85 M (EAT), and 302 M (EAT-large). For BEATs iter3 and EAT, input log-mel spectrograms are computed over 20–8000 Hz with frame length 25 and frame shift 10, then standardized using AudioSet statistics [9].

For Log-Mel, MFCC, BEATs, EAT, and EAT-large features, we use Temporal Mean Pooling ($Tmean$) over time, yielding 128-, 90-, 6144-, 6144-, and 8192-dimensional clip-level vectors, respectively. For EAT, we do not use the CLS embedding in order to preserve full band structure, unlike [13].

TABLE II
BEAM WINDOWING PARAMETERS (C : WINDOW DIM, s : STRIDE, N_b : NUMBER OF WINDOWS (BANDS)).

Feature	Dataset	(C, s)	N_b
Log-Mel	DCASE2020T2	(38, 38)	4
	DCASE2023T2	(38, 38)	4
	DCASE2024T2	(76, 76)	2
MFCC	All	(20, 20)	5
LPC spectrum	All	(3200, 3200)	3
BEATs [19]	All	(768, 768)	8
BEATs-FT	All	(768, 768)	8

2) *Proposed Training-Free Frontend System:* For Log-Mel, MFCC, and BEATs features, we use mean aggregation in the Dynamic Mean–Max module; this DMM variant is denoted *AdaBEAM*. In all cases except LPC spectrum, *BEAM* is applied to the $Tmean$ representation and can be combined with DMM to form *AdaBEAM*. The band/windowing parameters (C, s, N_b) for each feature type and dataset are summarized in Table II. For handcrafted features, we form bands by slicing the feature vector of length F (after temporal pooling when applicable) into length- C segments with stride s ; if $(F - C)$ is not divisible by s , we append one final *end-aligned* segment starting at $F - C$ (indices $[F - C, F)$), which may overlap with the preceding segment.

3) *Additional Finetuned Frontend System:* Under the same settings, we evaluate *BEAM* and *AdaBEAM* on fine-tuned BEATs encoders (SSL checkpoint iter3), adapting them to the target distribution using meta-information available from the reference normal data, following the AnoPatch recipe [8]. We perform full fine-tuning (updating all encoder parameters) with the AnoPatch outlier-exposure classification objective guided by this meta-information. To ensure reproducibility, we only instantiate the implementation choices that are not fully specified in [8] and do not tune them beyond the official development split: (i) audio preprocessing, where each segment is zero-padded or truncated to 10 s without standardization, enhancement, or segmentation; (ii) an attentive statistics pooling layer producing a 768-dimensional representation; and (iii) an ArcFace loss [84] with margin 0.5 and scale 64. All remaining hyperparameters follow [8] (or the AnoPatch public configuration, when available), and we perform no additional tuning.

Models are trained for 10k steps with a batch size of 32, gradient accumulation of 8, and the AdamW optimizer [85] with a learning rate of 1×10^{-4} and a linear scheduler (960 warm-up steps). Following the AnoPatch pipeline [8], we use SpecAugment [86] with a time mask of 80 and a frequency mask of 40 for DCASE2020T2, and a frequency mask of 80 for DCASE2023T2 and DCASE2024T2. Similar to [13], [21], classification targets correspond to machine sections in DCASE2020T2 and to machine attributions in DCASE2023T2 and DCASE2024T2, with 41, 167, and 141 classes, respectively. For simplicity and consistency, we use the same preprocessing as in the training-free frontend system.

We do not tune training hyperparameters, and instead follow the main settings from [8] for fair comparison. Nevertheless, frozen BEATs outperform fine-tuning on DCASE2023T2 and DCASE2024T2, consistent with [13]. Accordingly, we extract

TABLE III

COMPARISON OF OUR TRAINING-FREE FRONTEND SYSTEMS WITH PREVIOUSLY REPORTED RESULTS THAT DO NOT USE META-INFORMATION (AUXILIARY LABELS) FOR TRAINING OR FINE-TUNING. THIS SETTING ASSUMES ACCESS ONLY TO NORMAL DATA FROM THE SAME MACHINE TYPE (IN BOTH SOURCE AND TARGET DOMAINS); THUS TASK-SPECIFIC TRAINING ON NORMAL DATA (E.G., AE-STYLE METHODS) IS PERMITTED, WHILE METHODS THAT RELY ON AUXILIARY LABELS ARE EXCLUDED. OFFICIAL SCORES ARE REPORTED ON DCASE2020T2, DCASE2023T2, AND DCASE2024T2; WE USE THE ARITHMETIC MEAN (AMEAN) FOR DCASE2020T2 AND THE HARMONIC MEAN (HMEAN) FOR DCASE2023T2 AND DCASE2024T2.

Method	DCASE2020T2		DCASE2023T2 (DG)		DCASE2024T2 (DG)	
	sec-dev (Amean)	sec-eval (Amean)	sec-dev (Hmean)	sec-eval (Hmean)	sec-dev (Hmean)	sec-eval (Hmean)
Systems requiring task-specific training						
AE [5], [15], [16]	66.6	70.0	56.9	61.1	55.4	56.5
AE-IDNN [29]	71.5	-	-	-	-	-
ANP-IDNN [30]	71.8	75.6	-	-	-	-
PAE [31]	74.2	-	-	-	-	-
AudDSR [32]	78.2	-	-	-	-	-
UnlabeledASD [20] (PL)	-	-	63.5 ± 0.4	65.5 ± 0.5	-	-
Training-free systems (no task-specific training)						
<i>Handcrafted feature: Log-Mel</i>						
Global matching baseline	73.1	71.9	51.7	60.5	57.4	57.4
+ DMM	77.4 (+4.3)	74.9 (+3.0)	53.3 (+1.6)	61.9 (+1.4)	58.5 (+1.1)	58.0 (+0.6)
BEAM (proposed)	76.7 (+3.6)	75.4 (+3.5)	56.3 (+4.6)	67.8 (+7.3)	57.9 (+0.5)	57.9 (+0.5)
AdaBEAM (proposed)	80.6 (+7.5)	78.2 (+6.3)	56.9 (+5.2)	67.9 (+7.4)	58.5 (+1.1)	58.1 (+0.7)
<i>Handcrafted feature: MFCC</i>						
Global matching baseline	74.2	72.5	52.5	64.3	57.3	54.5
+ DMM	76.6 (+2.4)	76.4 (+3.9)	53.0 (+0.5)	63.4 (-0.9)	58.5 (+1.2)	53.8 (-0.7)
BEAM (proposed)	77.1 (+2.9)	75.4 (+2.9)	56.8 (+4.3)	64.8 (+0.5)	58.2 (+0.9)	56.6 (+2.1)
AdaBEAM (proposed)	77.6 (+3.4)	76.5 (+4.0)	57.0 (+4.5)	64.6 (+0.3)	58.7 (+1.4)	56.5 (+2.0)
<i>Handcrafted feature: LPC Spectrum</i>						
Global matching baseline	76.8	76.4	58.6	64.6	56.2	55.6
BEAM (proposed)	77.9 (+1.1)	80.0 (+3.6)	60.6 (+2.0)	66.2 (+1.6)	58.5 (+2.3)	57.3 (+1.7)
<i>Deep feature: EAT</i>						
Global matching baseline	77.8	77.7	61.3	66.0	57.1	58.9
+ DMM	78.5 (+0.7)	78.6 (+0.9)	61.6 (+0.3)	66.2 (+0.2)	57.3 (+0.2)	59.1 (+0.2)
BEAM (proposed)	84.3 (+6.5)	86.1 (+8.4)	63.9 (+2.6)	71.7 (+5.7)	60.2 (+3.1)	61.7 (+2.8)
AdaBEAM (proposed)	84.4 (+6.6)	86.5 (+8.8)	63.9 (+2.6)	71.5 (+5.5)	60.2 (+3.1)	61.7 (+2.8)
<i>Deep feature: EAT-Large</i>						
Global matching baseline (reported in [13])	79.3	79.9	65.0	66.1	56.8	58.9
Global matching baseline (our implementation)	78.2	78.0	61.5	64.7	56.8	59.8
+ DMM	79.1 (+0.9)	79.5 (+1.5)	61.9 (+0.4)	65.0 (+0.3)	57.3 (+0.5)	60.3 (+0.5)
BEAM (proposed)	84.2 (+6.0)	85.3 (+7.3)	64.0 (+2.5)	71.2 (+6.5)	59.8 (+3.0)	62.6 (+2.8)
AdaBEAM (proposed)	84.7 (+6.5)	86.1 (+8.1)	64.2 (+2.7)	71.1 (+6.4)	59.9 (+3.1)	63.0 (+3.2)
<i>Deep feature: BEATs-iter3</i>						
Global matching baseline (reported in [9])	74.7	-	-	73.8	-	-
Global matching baseline (reported in [13])	81.5	82.2	64.8	67.6	58.1	62.4
Global matching baseline (our implementation)	82.1	82.7	63.8	70.8	57.7	60.0
+ DMM	82.8 (+0.7)	83.9 (+1.2)	64.0 (+0.2)	70.9 (+0.1)	57.8 (+0.3)	61.7 (+1.7)
BEAM (proposed)	86.9 (+4.8)	87.8 (+5.1)	66.1 (+2.3)	73.1 (+2.3)	62.2 (+4.5)	62.6 (+2.6)
AdaBEAM (proposed)	87.6 (+5.5)	88.5 (+5.8)	66.3 (+2.5)	73.1 (+2.3)	62.4 (+4.7)	62.6 (+2.6)

embeddings from intermediate layers (layer 6 and layer 8, respectively) to mitigate pretraining–downstream mismatch [9]. Because sec-eval contains machine types absent from sec-dev in these DG benchmarks, we follow the sec-dev selection protocol in [13], yielding a first-shot setting where tuning uses disjoint machine types. For DCASE2020T2, we use the last layer by default.

4) *Anomaly Detector*: Following [13], we use $K = 1$ as the LDN neighborhood size in our main experiments. We also explore the effect of varying K for sub-band normalization (Section VII-B).

VII. RESULTS

Section VII-A presents the main training-free benchmark results on DCASE Task 2 (2020/2023/2024) under the im-

plementation described in Section VI-C, links the gains to variance reduction and sensitivity, and reports fine-tuned encoder performance as a secondary reference. Section VII-B then provides diagnostics on when the improvements hold, including the effects of sub-band window size, normalization neighborhood size K , and the roles of *BEAM* and *AdaBEAM*. Finally, Section VII-C presents a complementary MIMII study of clip-level feature behavior under varying noise conditions.

A. Main Results and Findings

Table III compares our training-free systems with previously reported results that do not use meta-information (i.e., auxiliary labels) for representation learning. Across DCASE Task 2 benchmarks, *BEAM* generally improved over tied-reference global matching across multiple front ends, with the largest

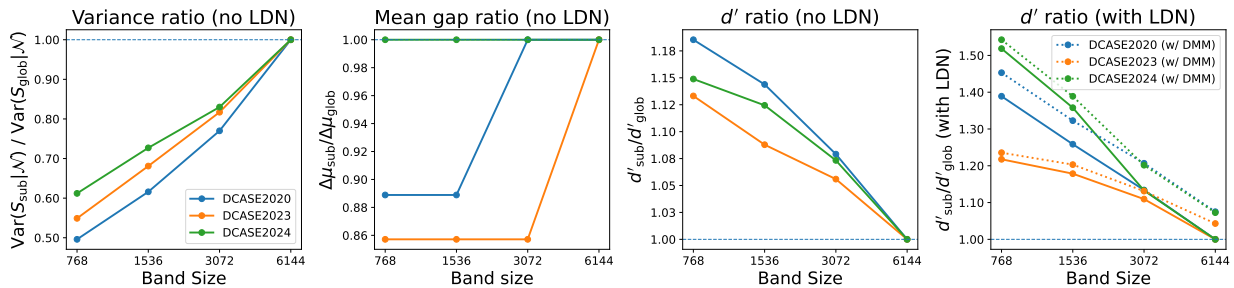


Fig. 2. Quantitative results for the theoretical analysis using BEATs iter3 features, averaged across machine types for each benchmark (DCASE2020T2, DCASE2023T2, and DCASE2024T2). (Left) Variance ratio (no LDN). (Center-left) Mean gap ratio (no LDN). (Center-right) d' ratio (no LDN). (Right) d' ratio with Local Density Normalization (LDN), including additional results with DMM.

TABLE IV

COMPARISON OF FINE-TUNED FRONTEND SYSTEMS THAT USE META-INFORMATION (AUXILIARY LABELS) DURING TASK-SPECIFIC TRAINING, TOGETHER WITH PREVIOUSLY REPORTED RESULTS FROM THE LITERATURE. OFFICIAL SCORES ARE REPORTED ON DCASE2020T2, DCASE2023T2, AND DCASE2024T2; SCORES FOR OUR APPROACH ARE AVERAGED OVER FIVE INDEPENDENT TRIALS. WE USE THE ARITHMETIC MEAN (AMEAN) FOR DCASE2020T2 AND THE HARMONIC MEAN (HMEAN) FOR DCASE2023T2 AND DCASE2024T2.

Method	DCASE2020T2		DCASE2023T2 (DG)		DCASE2024T2 (DG)	
	sec-dev (Amean)	sec-eval (Amean)	sec-dev (Hmean)	sec-eval (Hmean)	sec-dev (Hmean)	sec-eval (Hmean)
Prior work with global matching design						
SSL4ASD w/ LDN [12], [13]	90.7	90.2	68.4	68.0	62.0	54.7
+ 10 ensembles	94.2	93.3	71.3	72.4	65.2	56.5
AnoPatch [8](BEATs Full FT)	90.9	94.3	64.2	74.2	62.5 ± 0.8	65.6 ± 1.1
+ pseudo labeling [54]	-	-	-	-	64.1 ± 0.6	66.0 ± 0.7
AnoPatch-LoRA [53] (BEATs-LoRA)	-	-	67.3	77.2	-	-
UnlabeledASD [20]	-	-	67.2 ± 0.7	68.8 ± 0.9	-	-
ASDKit [21] (BEATs-LoRA)	90.6 ± 0.2	93.5 ± 0.3	62.7 ± 0.7	71.5 ± 0.5	59.5 ± 0.9	61.7 ± 0.7
This work (BEATs-iter3 Full FT)*						
Normalization: LDN (default)						
Global matching baseline	91.6 ± 0.2	93.0 ± 0.6	59.2 ± 0.5	71.9 ± 0.2	62.0 ± 1.2	57.8 ± 0.5
+ DMM	94.6 ± 0.1	95.2 ± 0.3	61.1 ± 0.1	72.0 ± 0.5	62.4 ± 0.4	57.0 ± 0.5
BEAM (proposed)	93.0 ± 0.3	94.0 ± 0.6	61.7 ± 0.4	75.3 ± 0.2	63.5 ± 0.5	59.4 ± 0.6
AdaBEAM (proposed)	95.6 ± 0.1	96.2 ± 0.2	63.1 ± 0.6	74.1 ± 0.6	62.9 ± 0.4	59.9 ± 0.7
Normalization: Domain-wise standardized scoring						
Global matching baseline	92.0 ± 0.1	93.9 ± 0.3	62.1 ± 0.3	75.5 ± 0.7	61.0 ± 0.7	63.1 ± 0.4
+ DMM	92.0 ± 0.1	93.7 ± 0.4	62.5 ± 0.3	75.4 ± 1.3	61.9 ± 0.5	63.5 ± 0.3
BEAM (proposed)	92.3 ± 0.1	93.8 ± 0.3	62.8 ± 0.1	76.4 ± 0.5	62.2 ± 0.4	62.9 ± 0.2
AdaBEAM (proposed)	92.2 ± 0.2	93.4 ± 0.5	63.4 ± 0.3	75.7 ± 0.7	62.9 ± 0.4	63.4 ± 0.2

*Averaged over five independent trials.

gains on BEATs features (see Sec. VII-B for further analysis). *AdaBEAM* further improved spectrogram-derived features by fusing temporal mean and temporal max views via DMM, although gains from the temporal-max view were limited in some settings (e.g., DCASE2023T2), indicating that temporal max pooling was not uniformly beneficial. DCASE2023T2 sec-eval was a notable exception, where the domain-wise score-normalization baseline [9] reported particularly strong results under a protocol with machine-type-specific layer selection. Handcrafted features also remained competitive with methods that relied on task-specific training while keeping the overall pipeline training-free. Overall, our method achieved strong training-free performance, improving over the global-matching design by a large margin on both handcrafted and deep neural front ends without machine-type-specific tuning.

Figure 2 provides empirical support for the SDT mechanism in Sec. IV on BEATs iter3 features using raw scores without LDN or DMM. Band-aligned sub-band matching with uniform

aggregation reduced the normal-score variance and increased sensitivity d' relative to tied-reference global matching. We directly evaluated the sufficient condition in Theorem 1 at each band size using the measured variance ratio and mean-gap ratio. The condition was satisfied at band sizes where the observed d' ratio $d'(S_{sub})/d'(S_{glob})$ exceeded one. At smaller band sizes, variance ratios dropped substantially while mean gap ratios remained close to one, and d' typically improved. As the band size increased, the gains diminished, approaching the global baseline. In some settings, sub-band matching slightly reduced the mean gap, but the accompanying reduction in normal spread was larger and d' still improved. Overall, these trends are consistent with our motivation: smaller sub-bands can reduce tied-reference mismatch via per-region reference selection, while uniform fusion can limit the influence of a few high-energy regions. We base this interpretation on the cross-frontend comparisons in Appendix C, which also suggest that most gains come from reducing tied-reference mismatch,

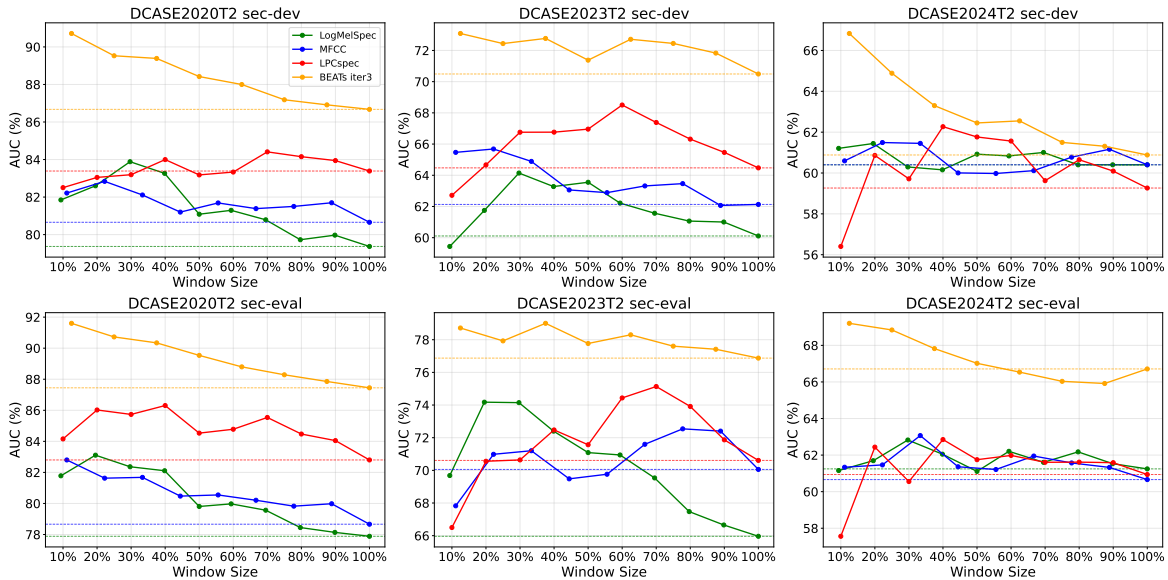


Fig. 3. Comparison of sub-band window sizes of *BEAM* on handcrafted and deep features (BEATs) in terms of AUC across DCASE2020T2, DCASE2023T2, and DCASE2024T2. Window size is reported as a fraction of the feature length along the windowed axis. For handcrafted features, we use non-overlapping windows for 10%–40% (stride equals window length); for 50%–90%, we use a two-window full-coverage rule with an end-aligned final window (equivalently, stride = $F - C$), which may overlap with the first window. For BEATs, windows are formed by grouping a fixed number of patch embeddings (8 patches total), thus only window sizes aligned to the patch grid are meaningful. Dotted horizontal lines show the baseline Tmean result.

while the effect of score fusion depends on the representation and band size.

Although LDN and DMM are not part of the theorem, we observed additional gains from applying LDN and from extending the scoring pipeline to DMM via *AdaBEAM*.

As a secondary reference, Table IV reports settings where task-specific training is feasible using auxiliary labels, with the BEATs encoder fine-tuned via the corresponding classification task. Fine-tuning improved performance over the training-free condition, and applying *BEAM* or DMM still provided additional gains over the fine-tuned global-matching baseline. Notably, training-free BEATs+*AdaBEAM* in Table III was already competitive with fine-tuned global-matching baselines on DCASE2023T2 and DCASE2024T2; for instance, it outperformed BEATs-LoRA [21] (spatial pooling) on DCASE2023T2 (66.3/73.1 vs. 62.7/71.5) and DCASE2024T2 (62.4/62.6 vs. 59.5/61.7). On DCASE2020T2, our fine-tuned *AdaBEAM* achieved Official Scores of 95.6 (sec-dev) and 96.2 (sec-eval), outperforming prior state-of-the-art systems, including SSL4ASD [13] (using 10 ensembles) and AnoPatch [8]. On DCASE2023T2 and DCASE2024T2, our fine-tuned results matched or slightly underperformed the strongest existing methods, with sec-dev/sec-eval discrepancies and LDN-related degradation on DCASE2024T2 sec-eval consistent with [13]. This indicates sensitivity to training strategy, so we report one fixed configuration (Section VI-C) and leave systematic tuning to future work. Applying Domain-Wise Standardized Scoring [9] avoided this effect and yielded stronger results, but it requires domain labels to handle domain shift.

B. Design Analysis

Effects of Dynamic Mean–Max Scoring. DMM compared scores from temporal mean and temporal max memory banks, testing whether transient events (captured by T_{max}) complemented stable, long-term statistics (captured by T_{mean}). In Table III, DMM yielded consistent gains over T_{mean} for k-NN+LDN across most feature types. When combined with sub-band matching (*AdaBEAM*), DMM typically provided an additional improvement over *BEAM* using T_{mean} alone, indicating that view fusion remained beneficial even after variance was reduced via sub-band reference selection.

Analysis of Sub-Band Window Sizes. Figure 3 analyzes the effect of sub-band granularity in *BEAM*. For handcrafted features, sub-band matching improved over the tied-reference global baseline across many window sizes, but the optimum was setting-dependent: very small windows (10%) underperformed in specific cases (e.g., LPC in some settings and MFCC on DCASE2023T2 sec-dev), whereas small-to-moderate windows were more consistently beneficial (Log-Mel/MFCC often around 20%–30%, LPC around 40%). BEATs showed a clearer trend, typically peaking at 10% and moving toward the global baseline as windows grew, with one exception on DCASE2024T2 sec-eval where large windows (60%–90%) underperformed. We attribute the stability of small windows for BEATs to patch-level invariances learned during large-scale pre-training, whereas handcrafted features can exhibit higher variance in fine partitions, which may over-suppress the mean gap and reduce d' (see Appendix Sec. C).

Impact of K for Sub-Band Density Scoring. Figure 4 shows how the neighborhood size K in sub-band density normalization affected Official Score for T_{mean}, T_{max}, and DMM variants using BEATs features. Across datasets, gains from LDN were dataset- and split-dependent and were typi-

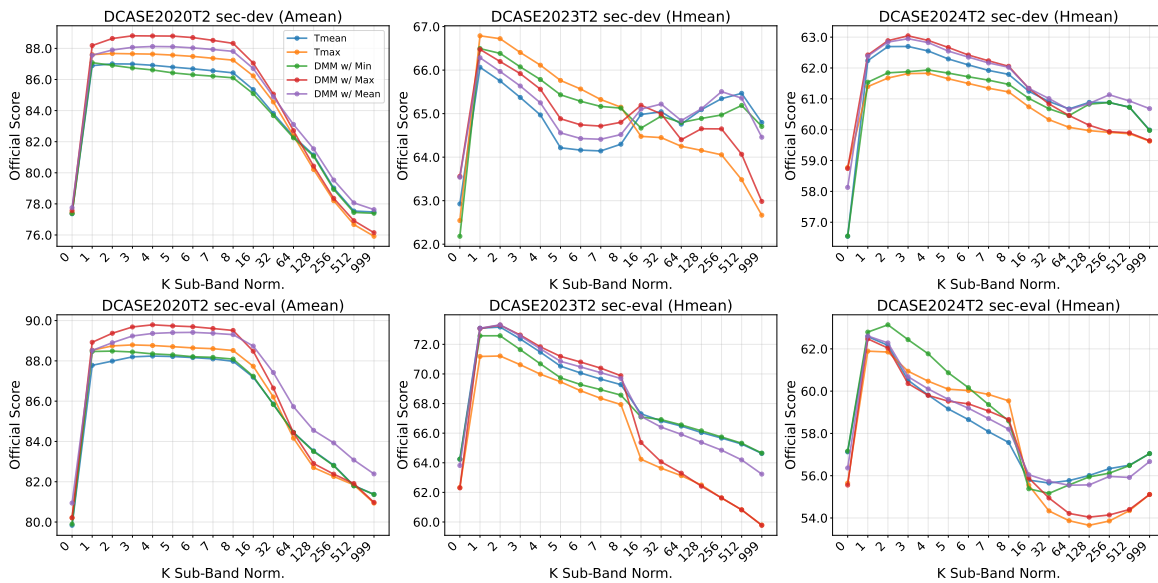


Fig. 4. Effect of varying K in sub-band density normalization on Official Scores across DCASE2020T2, DCASE2023T2, and DCASE2024T2. Results are shown for Tmean, Tmax, and DMM variants using BEATs features.

cally concentrated at small neighborhoods (around $K = 1-4$), while increasing K generally degraded performance. On DCASE2020T2, several methods improved when moving from $K = 1$ to $K = 2-4$; in contrast, on DCASE2023T2 sec-dev the best results were already attained at $K = 1$, and DCASE2023T2 sec-eval and DCASE2024T2 similarly favored very small K . We also observed a consistent interaction with DMM: as K grew, DMM with Max approached the Tmax branch and DMM with Min approached the Tmean branch, because large- K normalization reduced local-density variation and the aggregation rule effectively selected one of the two view-specific score distributions. Overall, DMM with Mean and DMM with Max appeared to perform consistently well across datasets relative to the other variants.

Sub-Band Scoring Strategy. Table V shows sub-band score aggregation rules for *BEAM* using BEATs features. Averaging across sub-bands consistently performed best, indicating that integrating evidence from all regions was more reliable than selecting a single extreme. Maximum aggregation was usually weaker than averaging, while minimum aggregation caused a substantial drop, suggesting that it could ignore anomalous regions by focusing on the easiest-matching sub-band. Comparing *BEAM* applied to temporal mean vs. temporal max memory banks further showed that each view could be preferable depending on the dataset; combining them with DMM (mean aggregation) therefore provided the most robust overall scoring.

C. MIMII: Clip-Level Feature Analysis

We analyzed clip-level representations on the MIMII dataset [3], which included both stationary (Fan, Pump) and non-stationary (Slider, Valve) machine types under varying SNR conditions. Figure 5 compares different front ends using tied-reference global matching (standard k -NN without applying local density normalization [9]). Among the evaluated

TABLE V
COMPARISON OF DIFFERENT *BEAM* SUB-BAND SCORING APPROACHES USING BEATs FEATURES. HIGHER OFFICIAL SCORES INDICATE BETTER PERFORMANCE.

Method	DCASE2020T2		DCASE2023T2 (DG)		DCASE2024T2 (DG)	
	sec-dev	sec-eval	sec-dev	sec-eval	sec-dev	sec-eval
<i>Baseline w/o Local Density Normalization (apply [9])</i>						
Tmean	75.8	77.5	62.6	71.7	56.3	59.0
w/ Sub-Band						
Average	77.5	80.3	63.1	72.7	59.4	60.0
Maximum	78.0	80.7	62.7	69.9	57.3	59.4
Minimum	69.9	71.5	60.7	66.2	56.1	56.0
Sub-Band Tmean						
Average	86.9	87.8	66.1	73.1	62.2	62.6
Maximum	84.0	85.4	61.7	72.4	62.1	61.4
Minimum	78.1	78.9	63.5	66.1	59.9	58.3
Sub-Band Tmax						
Average	87.5	88.5	66.8	71.2	61.3	61.9
Maximum	84.8	86.7	61.2	69.5	61.8	60.4
Minimum	76.9	78.2	63.4	65.6	57.3	57.5
Sub-Band DMM w/ Min						
Average	87.0	88.4	66.5	72.6	61.4	62.8
Maximum	85.3	87.2	61.7	69.8	62.0	61.1
Minimum	77.8	78.6	63.3	67.2	59.9	58.5
Sub-Band DMM w/ Max						
Average	88.1	88.8	66.5	73.0	62.2	61.5
Maximum	84.8	87.5	60.7	72.9	62.2	59.9
Minimum	79.7	81.1	64.3	67.1	58.7	58.5
Sub-Band DMM w/ Mean						
Average	87.6	88.5	66.3	73.1	62.4	62.6
Maximum	83.9	84.5	63.1	72.6	62.1	62.5
Minimum	79.3	80.5	63.9	66.9	59.8	58.6

handcrafted features, the LPC spectrum performed particularly well and, in this setting, even surpassed deep BEATs features. We also found that temporal max pooling consistently outperformed temporal mean pooling, highlighting the importance of retaining transient information for non-stationary machines.

These trends can be explained by how LPC relates to conventional spectral features. Like max-pooled Log-Mel or MFCCs, LPC emphasized prominent spectral peaks while modeling a smooth spectral envelope that captured longer-

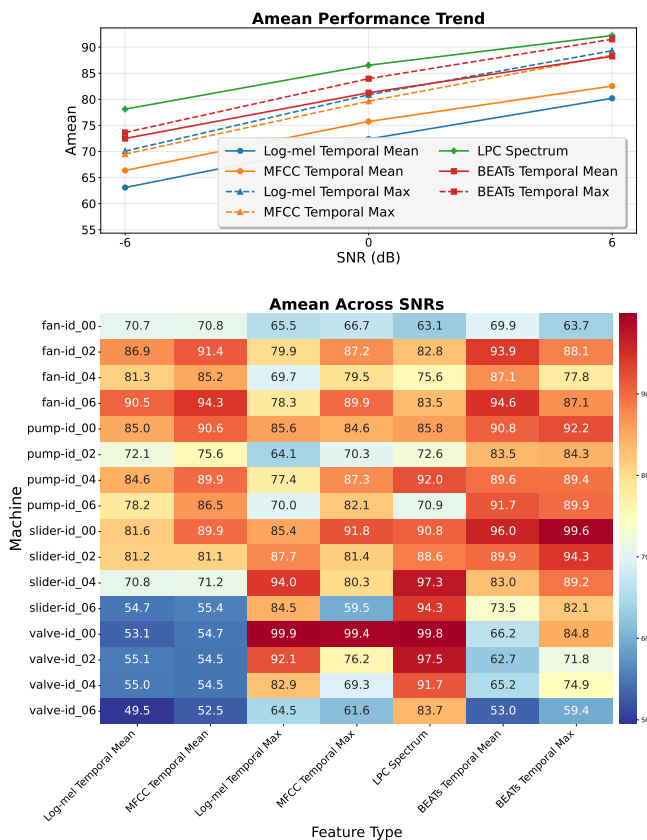


Fig. 5. Comparison of features on the MIMII dataset.

TABLE VI

COMPUTATIONAL COST PER 10 S CLIP (MEAN \pm STD OVER $n_{\text{runs}} = 5$). FEATURE-EXTRACTION TIME MEASURES WAVEFORM \rightarrow F, AND END-TO-END (E2E) TIME MEASURES WAVEFORM \rightarrow ANOMALY SCORE, INCLUDING 1-NN SCORING AGAINST A MEMORY BANK OF 500 NORMAL CLIPS. HANDCRAFTED FRONTENDS ARE COMPUTED ON CPU ONLY IN THIS BENCHMARK. CPU: AMD RYZEN 5 5600X. GPU: NVIDIA GEFORCE RTX 3090. FOR BEATs, THE ENCODER COMPLEXITY IS REPORTED AS MACs/PARAMS (G/M).

Frontend	Output dim	Feat. (ms)	E2E (ms)	MACs/Params (G/M)
Log-Mel (Tmean)	128	3.95 \pm 0.21	6.20 \pm 0.25	N/A
MFCC (Tmean)	90	3.95 \pm 0.01	7.95 \pm 1.08	N/A
LPC spectrum	8000	31.34 \pm 0.05	41.11 \pm 0.15	N/A
BEATs iter3 (Tmean, CPU)	6144	271.15 \pm 6.06	494.02 \pm 6.19	45.01/90.71
BEATs iter3 (Tmean, GPU)	6144	13.60 \pm 0.14	17.91 \pm 0.14	45.01/90.71

term structure in stationary sounds. At the same time, because LPC estimated a global envelope, it could be more sensitive to background noise in low-SNR stationary conditions, where band-wise energy integration and smoothing with Log-Mel or MFCCs could be more robust. Overall, LPC-based representations offered a complementary trade-off: they could outperform pooled Log-Mel and MFCC baselines while remaining lightweight, non-parametric, and interpretable by revealing frequency regions where anomalies occurred.

Table VI reports per-clip inference cost from waveform to anomaly score. Handcrafted front ends were inexpensive on CPU: Log-Mel and MFCC required single-digit milliseconds end-to-end, and LPC-based features required tens of milliseconds. BEATs was about two orders of magnitude slower on CPU due to neural-encoder inference (45.01 G

MACs, 90.71 M parameters) and reached comparable latency only on GPU. Together with the MIMII results (Figure 5) and the main benchmark results (Table III), these numbers indicate that handcrafted representations remained competitive in the training-free setting while providing a strong efficiency baseline for CPU-only deployments.

VIII. CONCLUSION

We present *BEAM*, a band-aligned sub-band matching framework for anomalous sound detection (ASD) that replaces tied-reference global matching with a shared memory of sub-band embeddings, per-band nearest-neighbor retrieval, and uniform aggregation across sub-bands. This design targets two sources of inflated normal-score variance: tied-reference mismatch under band-wise variability and implicit energy weighting that lets a few high-energy bands dominate matching and aggregation. Across both handcrafted and deep neural front ends, *BEAM* improved over tied-reference global matching and achieved strong training-free performance on DCASE Task 2 benchmarks, while remaining competitive with methods that require task-specific training. Our SDT analysis provided a sufficient condition under which variance reduction, without excessive mean-gap loss, improved detection sensitivity. For spectrogram-based features, *AdaBEAM* extended *BEAM* by fusing mean- and max-pooled views through a parameter-free Dynamic Mean–Max rule, indicating that combining complementary stationary and transient cues can further improve sensitivity and performance. Overall, sub-band memory modeling with localized scoring provides a practical alternative to tied-reference global matching for fine-grained ASD.

The main benchmark comparisons were conducted under a fixed implementation protocol without exhaustive hyperparameter tuning, while our analysis suggests that additional gains may be achievable by tuning handcrafted-feature windowing and sub-band normalization neighborhood size K for each dataset (and, where appropriate, machine setup). These findings suggest possible future directions centered on adaptive band partitioning and improved score calibration for machine-specific tuning.

ACKNOWLEDGMENTS

This work was supported by JTEKT Corporation.

APPENDIX

This appendix explains, in the SDT sense, when the proposed sub-band score can achieve higher sensitivity d' than exact global cosine matching. We define the proposed sub-band score S_{sub} , the baseline global score S_{glob} , and an analytic proxy S_{uni} that uses uniform band aggregation (as in S_{sub}) while tying all bands to the global reference index (as in S_{glob}). We then bound the normal-class variance of S_{sub} relative to S_{glob} and combine it with an exact mean-gap identity to give a sufficient condition for $d'(S_{\text{sub}}) \geq d'(S_{\text{glob}})$.

A. Theoretical setup and definitions

a) *Objective and SDT convention.*: Let y denote a test sample drawn from either the normal class \mathcal{N} or anomalous class \mathcal{A} . All quantities below (scores, indices, weights) are random variables defined as measurable functions of y . For any real-valued score $S(y)$, define

$$d'(S) \triangleq \frac{\Delta(S)}{\sqrt{\text{Var}(S | \mathcal{N})}}, \quad \Delta(S) \triangleq \mathbb{E}[S | \mathcal{A}] - \mathbb{E}[S | \mathcal{N}],$$

where $\mathbb{E}[\cdot | \mathcal{C}]$ and $\text{Var}(\cdot | \mathcal{C})$ denote expectation and variance under the conditional distribution of y given class $\mathcal{C} \in \{\mathcal{N}, \mathcal{A}\}$. We assume the scoring direction is calibrated so that larger scores indicate ‘‘more anomalous’’ and focus on the regime $\Delta(S) > 0$.

b) *Feature decomposition and cosine conventions.*: Let the test feature be a concatenation of N_b sub-vectors (sub-bands) $f_y = (w_{y,1}, \dots, w_{y,N_b})$, where $w_{y,j} \in \mathbb{R}^{d_j}$. We index normal reference clips by $\mathcal{M}_{\text{glob}} = \{1, \dots, R\}$ and write each normal template as $f_i = (w_{i,1}, \dots, w_{i,N_b})$ for $i \in \mathcal{M}_{\text{glob}}$. For each band j , the corresponding band-aligned memory bank is $\mathcal{M}_j \triangleq \{w_{i,j}\}_{i \in \mathcal{M}_{\text{glob}}}$, and sub-band matching selects templates within the same band j . We interpret concatenation in orthogonal coordinate blocks, so that

$$\langle f_y, f_i \rangle = \sum_{j=1}^{N_b} \langle w_{y,j}, w_{i,j} \rangle, \quad \|f_y\|^2 = \sum_{j=1}^{N_b} \|w_{y,j}\|^2.$$

Define cosine similarity with the standard convention, extended at zero norm by

$$\cos(a, b) \triangleq \begin{cases} \frac{\langle a, b \rangle}{\|a\| \|b\|}, & \|a\| \|b\| > 0, \\ 0, & \|a\| \|b\| = 0, \end{cases}$$

and the cosine distance

$$D(a, b) \triangleq \frac{1}{2}(1 - \cos(a, b)) \in [0, 1].$$

c) *Globally selected reference (with deterministic tie-breaking).*: Define the global reference index by picking the smallest index among the maximizers:

$$i^*(y) \triangleq \min \arg \max_{i \in \mathcal{M}_{\text{glob}}} \cos(f_y, f_i).$$

Since $\mathcal{M}_{\text{glob}}$ is finite and the tie-breaking rule is deterministic, $i^*(y)$ is well-defined and measurable.

d) *Per-band similarities and distances.*: Define the per-band cosine similarity w.r.t. the globally selected template

$$s_j(y) \triangleq \cos(w_{y,j}, w_{i^*(y),j}),$$

and the per-band cosine distance to any template

$$D_{j,i}(y) \triangleq D(w_{y,j}, w_{i,j}) = \frac{1}{2}(1 - \cos(w_{y,j}, w_{i,j})).$$

e) *Sub-band score.*: This score allows *per-band template selection* within the band-aligned memory: for each band j , we minimize over references $i \in \mathcal{M}_j$ when computing the cosine distance, and aggregate the resulting per-band distances uniformly:

$$S_{\text{sub}}(y) \triangleq \frac{1}{N_b} \sum_{j=1}^{N_b} \min_{i \in \mathcal{M}_j} D_{j,i}(y).$$

f) *Uniform tied-reference proxy.*: This proxy ties all bands to the same globally selected reference $i^*(y)$ and aggregates per-band distances uniformly, defined by

$$S_{\text{uni}}(y) \triangleq \frac{1}{N_b} \sum_{j=1}^{N_b} D_{j,i^*(y)}(y) = \frac{1}{2} \left(1 - \frac{1}{N_b} \sum_{j=1}^{N_b} s_j(y) \right).$$

g) *Exact global cosine score (baseline).*: Define the band-energy coupling weights

$$\beta_j(y) \triangleq \begin{cases} \frac{\|w_{y,j}\| \|w_{i^*(y),j}\|}{\|f_y\| \|f_{i^*(y)}\|}, & \|f_y\| \|f_{i^*(y)}\| > 0, \\ 0, & \|f_y\| \|f_{i^*(y)}\| = 0, \end{cases}$$

$$\rho(y) \triangleq \sum_{j=1}^{N_b} \beta_j(y) \leq 1.$$

When $\|f_y\| \|f_{i^*(y)}\| > 0$, $\rho(y) \leq 1$ follows from Cauchy–Schwarz: $\sum_{j=1}^{N_b} \|w_{y,j}\| \|w_{i^*(y),j}\| \leq \|f_y\| \|f_{i^*(y)}\|$; otherwise $\rho(y) = 0$. Define normalized weights

$$\tilde{\beta}_j(y) \triangleq \begin{cases} \beta_j(y)/\rho(y), & \rho(y) > 0, \\ 1/N_b, & \rho(y) = 0, \end{cases} \quad \sum_{j=1}^{N_b} \tilde{\beta}_j(y) = 1.$$

Then the exact global cosine distance to the selected template is

$$\begin{aligned} S_{\text{glob}}(y) &\triangleq \frac{1}{2} \left(1 - \cos(f_y, f_{i^*(y)}) \right) \\ &= \frac{1}{2} \left(1 - \rho(y) \sum_{j=1}^{N_b} \tilde{\beta}_j(y) s_j(y) \right). \end{aligned}$$

h) *Two deviation terms and their class-conditional gaps.*: We define two auxiliary quantities that isolate how S_{sub} and S_{glob} differ from the common proxy S_{uni} : the per-band selection gain P and the energy-weighting deviation B .

Define the tied-index mismatch penalty

$$P(y) \triangleq S_{\text{uni}}(y) - S_{\text{sub}}(y) \geq 0,$$

where $P(y) \geq 0$ holds since $\min_{i \in \mathcal{M}_j} D_{j,i}(y) \leq D_{j,i^*(y)}(y)$ for each j . Define the energy-weighting deviation

$$B(y) \triangleq \rho(y) \sum_{j=1}^{N_b} \tilde{\beta}_j(y) s_j(y) - \frac{1}{N_b} \sum_{j=1}^{N_b} s_j(y).$$

By construction, the following pointwise identities hold for all y :

$$S_{\text{sub}}(y) = S_{\text{uni}}(y) - P(y), \quad S_{\text{glob}}(y) = S_{\text{uni}}(y) - \frac{1}{2} B(y).$$

Define class-conditional gaps

$$\Delta P \triangleq \mathbb{E}[P | \mathcal{A}] - \mathbb{E}[P | \mathcal{N}], \quad \Delta B \triangleq \mathbb{E}[B | \mathcal{A}] - \mathbb{E}[B | \mathcal{N}].$$

i) *Regime descriptor.*: Let \mathcal{G} be a coarse sigma-field (a regime descriptor) such that pipeline outputs that may affect variability are \mathcal{G} -measurable (e.g., $i^*(y)$, $\rho(y)$, coarse bins of $\tilde{\beta}(y)$, operating-condition labels, etc.). We condition on \mathcal{G} to apply the law of total variance under \mathcal{N} . We will use \mathcal{G} to decompose within-regime and between-regime variance under \mathcal{N} . We assume \mathcal{G} is fixed a priori as an operating-regime descriptor and is not so rich that it determines S_{uni} , i.e., $\mathbb{E}[\text{Var}(S_{\text{uni}} | \mathcal{G}, \mathcal{N}) | \mathcal{N}] > 0$.

B. Variance effects and discriminability of the two mechanisms

Proposition 1 (Normal-variance ratio from per-sub-band selection and global aggregation). *Under the normal class \mathcal{N} , we upper-bound $\text{Var}(S_{\text{sub}} | \mathcal{N})$ by a constant multiple of $\text{Var}(S_{\text{glob}} | \mathcal{N})$. The constant separates the effects of (i) per-band template selection versus a tied global reference and (ii) uniform aggregation versus energy-coupled global aggregation. Assume all variances/covariances below are finite and $\text{Var}(S_{\text{glob}} | \mathcal{N}) > 0$.*

Let \mathcal{G} be a coarse sigma-field (regime descriptor) such that

$$\begin{aligned} 0 &< \mathbb{E}[\text{Var}(S_{\text{uni}} | \mathcal{G}, \mathcal{N}) | \mathcal{N}] < \infty, \\ 0 &< \mathbb{E}[\text{Var}(S_{\text{glob}} | \mathcal{G}, \mathcal{N}) | \mathcal{N}] < \infty. \end{aligned}$$

Define

$$\begin{aligned} g_0 &\triangleq \frac{\mathbb{E}[\text{Var}(S_{\text{glob}} | \mathcal{G}, \mathcal{N}) | \mathcal{N}]}{\mathbb{E}[\text{Var}(S_{\text{uni}} | \mathcal{G}, \mathcal{N}) | \mathcal{N}]}, \\ \gamma &\triangleq \frac{\text{Var}(\mathbb{E}[S_{\text{uni}} | \mathcal{G}, \mathcal{N}] | \mathcal{N})}{\mathbb{E}[\text{Var}(S_{\text{uni}} | \mathcal{G}, \mathcal{N}) | \mathcal{N}]}. \end{aligned}$$

Define

$$\begin{aligned} p_0 &\triangleq \frac{\text{Var}(P | \mathcal{N})}{\text{Var}(S_{\text{glob}} | \mathcal{N})} \geq 0, \\ \lambda &\triangleq \left(\frac{-2 \text{Cov}(S_{\text{sub}}, P | \mathcal{N})}{\text{Var}(S_{\text{glob}} | \mathcal{N})} \right)_+, \quad (x)_+ \triangleq \max\{x, 0\}. \end{aligned}$$

By construction, $\lambda \geq 0$ and $-2 \text{Cov}(S_{\text{sub}}, P | \mathcal{N}) \leq \lambda \text{Var}(S_{\text{glob}} | \mathcal{N})$.

Let

$$C_{\text{var}} \triangleq \frac{1 + \gamma}{g_0} + \lambda - p_0. \quad (11)$$

Note that $(1 + \gamma)/g_0 > 0$ and $\lambda \geq 0$, thus $C_{\text{var}} \geq 0$ fails only if p_0 is large enough to make $\frac{1 + \gamma}{g_0} + \lambda - p_0 < 0$. Assume $C_{\text{var}} \geq 0$ so that the refined variance factor is nonnegative. Then

$$\text{Var}(S_{\text{sub}} | \mathcal{N}) \leq C_{\text{var}} \text{Var}(S_{\text{glob}} | \mathcal{N}). \quad (12)$$

Proof. Under \mathcal{N} , we have the pointwise decomposition $S_{\text{uni}} = S_{\text{sub}} + P$, hence

$$\begin{aligned} \text{Var}(S_{\text{uni}} | \mathcal{N}) &= \text{Var}(S_{\text{sub}} | \mathcal{N}) + \text{Var}(P | \mathcal{N}) \\ &\quad + 2 \text{Cov}(S_{\text{sub}}, P | \mathcal{N}), \end{aligned}$$

and therefore

$$\begin{aligned} \text{Var}(S_{\text{sub}} | \mathcal{N}) &= \text{Var}(S_{\text{uni}} | \mathcal{N}) - \text{Var}(P | \mathcal{N}) \\ &\quad - 2 \text{Cov}(S_{\text{sub}}, P | \mathcal{N}). \end{aligned}$$

By the definition of λ ,

$$-2 \text{Cov}(S_{\text{sub}}, P | \mathcal{N}) \leq \lambda \text{Var}(S_{\text{glob}} | \mathcal{N}),$$

so

$$\begin{aligned} \text{Var}(S_{\text{sub}} | \mathcal{N}) &\leq \text{Var}(S_{\text{uni}} | \mathcal{N}) - \text{Var}(P | \mathcal{N}) \\ &\quad + \lambda \text{Var}(S_{\text{glob}} | \mathcal{N}). \end{aligned} \quad (13)$$

Next, by the law of total variance under \mathcal{N} ,

$$\begin{aligned} \text{Var}(S_{\text{glob}} | \mathcal{N}) &= \mathbb{E}[\text{Var}(S_{\text{glob}} | \mathcal{G}, \mathcal{N}) | \mathcal{N}] + \text{Var}(\mathbb{E}[S_{\text{glob}} | \mathcal{G}, \mathcal{N}] | \mathcal{N}) \\ &\geq \mathbb{E}[\text{Var}(S_{\text{glob}} | \mathcal{G}, \mathcal{N}) | \mathcal{N}] = g_0 \mathbb{E}[\text{Var}(S_{\text{uni}} | \mathcal{G}, \mathcal{N}) | \mathcal{N}], \end{aligned} \quad (15)$$

where the last equality is the definition of g_0 . Similarly,

$$\begin{aligned} \text{Var}(S_{\text{uni}} | \mathcal{N}) &= \mathbb{E}[\text{Var}(S_{\text{uni}} | \mathcal{G}, \mathcal{N}) | \mathcal{N}] + \text{Var}(\mathbb{E}[S_{\text{uni}} | \mathcal{G}, \mathcal{N}] | \mathcal{N}) \\ &= (1 + \gamma) \mathbb{E}[\text{Var}(S_{\text{uni}} | \mathcal{G}, \mathcal{N}) | \mathcal{N}], \end{aligned} \quad (16)$$

where the last equality is the definition of γ .

Combining (14) and (16) yields

$$\text{Var}(S_{\text{uni}} | \mathcal{N}) \leq \frac{1 + \gamma}{g_0} \text{Var}(S_{\text{glob}} | \mathcal{N}). \quad (18)$$

Plugging (18) into (13) gives

$$\text{Var}(S_{\text{sub}} | \mathcal{N}) \leq \left(\frac{1 + \gamma}{g_0} + \lambda \right) \text{Var}(S_{\text{glob}} | \mathcal{N}) - \text{Var}(P | \mathcal{N}).$$

Since $\text{Var}(P | \mathcal{N}) = p_0 \text{Var}(S_{\text{glob}} | \mathcal{N})$, we obtain

$$\text{Var}(S_{\text{sub}} | \mathcal{N}) \leq \left(\frac{1 + \gamma}{g_0} + \lambda - p_0 \right) \text{Var}(S_{\text{glob}} | \mathcal{N}).$$

Since $C_{\text{var}} \geq 0$ by assumption, this proves (12) with C_{var} defined in (11).

Theorem 1 (Sufficient condition for d' improvement). *Assume $\Delta(S_{\text{glob}}) > 0$ and $\text{Var}(S_{\text{glob}} | \mathcal{N}) > 0$. Assume also $\text{Var}(S_{\text{sub}} | \mathcal{N}) > 0$. Assume the normal-variance bound from Proposition 1:*

$$\text{Var}(S_{\text{sub}} | \mathcal{N}) \leq C_{\text{var}} \text{Var}(S_{\text{glob}} | \mathcal{N}),$$

where $C_{\text{var}} \geq 0$ is defined in (11). Let $\eta \triangleq \sqrt{C_{\text{var}}}$ (thus $\eta > 0$ under the assumptions above). If the mean-gap compatibility condition

$$\Delta(S_{\text{glob}}) + \frac{1}{2} \Delta B - \Delta P \geq \eta \Delta(S_{\text{glob}}) \quad (19)$$

holds (equivalently, $\Delta P - \frac{1}{2} \Delta B \leq (1 - \eta) \Delta(S_{\text{glob}})$), then

$$d'(S_{\text{sub}}) \geq d'(S_{\text{glob}}).$$

Proof. Using $d'(S) = \Delta(S) / \sqrt{\text{Var}(S | \mathcal{N})}$,

$$\frac{d'(S_{\text{sub}})}{d'(S_{\text{glob}})} = \frac{\Delta(S_{\text{sub}})}{\Delta(S_{\text{glob}})} \cdot \sqrt{\frac{\text{Var}(S_{\text{glob}} | \mathcal{N})}{\text{Var}(S_{\text{sub}} | \mathcal{N})}}.$$

To show this ratio is at least 1, it suffices to find $\eta > 0$ such that

$$\frac{\Delta(S_{\text{sub}})}{\Delta(S_{\text{glob}})} \geq \eta \quad \text{and} \quad \sqrt{\frac{\text{Var}(S_{\text{glob}} | \mathcal{N})}{\text{Var}(S_{\text{sub}} | \mathcal{N})}} \geq \frac{1}{\eta},$$

because then multiplying the two bounds gives

$$\frac{d'(S_{\text{sub}})}{d'(S_{\text{glob}})} \geq \eta \cdot \frac{1}{\eta} = 1.$$

The second inequality above is equivalent to $\text{Var}(S_{\text{sub}} | \mathcal{N}) \leq \eta^2 \text{Var}(S_{\text{glob}} | \mathcal{N})$, which holds by the assumed bound with $\eta = \sqrt{C_{\text{var}}}$.

For the first inequality, use the pointwise identities $S_{\text{sub}} = S_{\text{uni}} - P$ and $S_{\text{glob}} = S_{\text{uni}} - \frac{1}{2}B$ to obtain

$$S_{\text{sub}} - S_{\text{glob}} = \frac{1}{2}B - P.$$

Taking class-conditional expectations and subtracting gives the exact mean-gap identity

$$\Delta(S_{\text{sub}}) - \Delta(S_{\text{glob}}) = \frac{1}{2} \Delta B - \Delta P,$$

$$\text{equivalently, } \Delta(S_{\text{sub}}) = \Delta(S_{\text{glob}}) + \frac{1}{2} \Delta B - \Delta P.$$

Thus the compatibility condition (19) is exactly $\Delta(S_{\text{sub}}) \geq \eta \Delta(S_{\text{glob}})$, which is the first inequality needed. Combining the two inequalities yields $d'(S_{\text{sub}}) \geq d'(S_{\text{glob}})$.

Interpretation. Intuitively, sub-band matching can improve d' when it reduces normal-class variability more than it erodes the normal-anomalous mean separation. Proposition 1 formalizes the first part by bounding $\text{Var}(S_{\text{sub}} | \mathcal{N}) \leq C_{\text{var}} \text{Var}(S_{\text{glob}} | \mathcal{N})$ with $C_{\text{var}} = ((1 + \gamma)/g_0 + \lambda - p_0)$. The factor $(1 + \gamma)/g_0$ quantifies the change in normal variability when replacing energy-coupled global cosine aggregation (S_{glob}) by uniform band aggregation (S_{uni}) across operating conditions summarized by \mathcal{G} , while $(\lambda - p_0)$ captures the effect of per-band template selection relative to a tied global reference through the mismatch penalty P and its covariance term. Theorem 1 gives a sufficient condition for d' improvement provided the mean gap is not reduced beyond the variance gain, namely $\Delta(S_{\text{sub}}) \geq \eta \Delta(S_{\text{glob}})$ with $\eta = \sqrt{C_{\text{var}}}$. Using $\Delta(S_{\text{sub}}) = \Delta(S_{\text{glob}}) + \frac{1}{2} \Delta B - \Delta P$, this condition becomes $\Delta(S_{\text{glob}}) + \frac{1}{2} \Delta B - \Delta P \geq \eta \Delta(S_{\text{glob}})$, where ΔP is the cost of enforcing a single global reference and ΔB is the mean shift from removing energy-weighted coupling in the global cosine. LDN rescales each raw band-wise distance by a local scale statistic around the selected memory item (e.g., a k -NN radius), which can reduce sensitivity to band- or condition-dependent multiplicative distance scaling under \mathcal{N} and make band scores more comparable before uniform averaging; the same derivation then carries through Theorem 1 after replacing $D_{j,i}(y)$ by its LDN-normalized counterpart, with LDN entering only through the resulting variance and mean-gap terms.

C. Additional results on sensitivity analysis

Table VII reveals distinct d' trends among band-preserved features, contrasting BEATs with handcrafted representations (Log-Mel and LPC spectrum). BEATs consistently exhibits peak d' at the smallest band size, corresponding to temporally pooled patch-level embeddings, and gradually regresses toward the global baseline (i.e., the largest band size) as band size increases. This behavior is consistent with the invariance properties induced by large-scale pre-training, which reduce sensitivity to nuisance factors such as noise and operating-condition shifts even at very fine partitions. In contrast, Log-Mel and LPC generally achieve peak d' at small-to-medium band sizes, indicating a different balance between variance suppression and mean-gap behavior.

These differences can be explained by the interaction between tied-reference mismatch, energy-weighted aggregation, and overall variance suppression as band size varies. For BEATs, sub-band matching primarily reduces variance by alleviating tied-reference mismatch, reflected in $\text{Var}(S_{\text{sub}} | \mathcal{N})/\text{Var}(S_{\text{uni}} | \mathcal{N}) < 1$, while the anomaly mean gap

remains close to the global baseline, so improvements in d' are variance-driven. Suppression of energy-dominant aggregation, captured by $\text{Var}(S_{\text{uni}} | \mathcal{N})/\text{Var}(S_{\text{glob}} | \mathcal{N})$, is most pronounced on the domain-generalization (DG) datasets for both BEATs and Log-Mel, although BEATs remains relatively stable across band sizes. Log-Mel benefits from both reduced mismatch and mitigation of energy-dominant aggregation, but at very fine partitions the overall variance term $\text{Var}(S_{\text{sub}} | \mathcal{N})/\text{Var}(S_{\text{glob}} | \mathcal{N})$ can be over-suppressed and the mean gap collapses, leading to non-monotonic d' behavior. In contrast, LPC is dominated by the tied-reference mechanism: aggregation effects are weak or even adverse, yet d' still increases because sub-band matching suppresses mismatch-driven normal-score variance and simultaneously increases the anomaly mean gap, as envelope distortions caused by faults are more localized and structurally consistent within the same sub-bands than the diffuse, band-inconsistent fluctuations observed under normal operation.

Overall, these observations are consistent with our Theorem 1, which predict that sensitivity improvements arise when reductions in normal-score variance are not offset by a corresponding collapse in the anomaly mean gap. Sub-band matching systematically promotes this regime, explaining its consistent gains in d' across feature types, despite their differing spectral and statistical properties.

REFERENCES

- [1] Y. Koizumi, S. Saito, H. Uematsu, and N. Harada, "Optimizing acoustic feature extractor for anomalous sound detection based on neyman-pearson lemma," in *Proc. EUSIPCO*, 2017, pp. 698–702.
- [2] H. Uematsu, Y. Koizumi, S. Saito, A. Nakagawa, and N. Harada, "Anomaly detection technique in sound to detect faulty equipment," *NTT Technical Review*, 2017.
- [3] H. Purohit, R. Tanabe *et al.*, "MIMII Dataset: Sound dataset for malfunctioning industrial machine investigation and inspection," in *Proc. DCASE*, 2019, pp. 209–213.
- [4] Y. Koizumi, S. Saito, H. Uematsu, N. Harada, and K. Imoto, "ToyADMOS: A dataset of miniature-machine operating sounds for anomalous sound detection," in *Proc. WASPAA*, 2019, pp. 308–312.
- [5] Y. Koizumi, Y. Kawaguchi *et al.*, "Description and Discussion on DCASE2020 Challenge Task2: Unsupervised Anomalous Sound Detection for Machine Condition Monitoring," in *Proc. DCASE*. arXiv, 2020.
- [6] V. Chandola, A. Banerjee, and V. Kumar, "Anomaly detection: A survey," *ACM CSUR*, vol. 41, no. 3, pp. 1–58, 2009.
- [7] K. Wilkinghoff, "Audio embeddings for semi-supervised anomalous sound detection," Ph.D. dissertation, University of Bonn, 2024.
- [8] A. Jiang, B. Han *et al.*, "Anopatch: Towards better consistency in machine anomalous sound detection," in *Proc. Interspeech*, 2024.
- [9] P. Saengthong and T. Shinozaki, "Deep generic representations for domain-generalized anomalous sound detection," in *Proc. ICASSP*, 2025, pp. 1–5.
- [10] —, "Genrep for first-shot unsupervised anomalous sound detection of dcase 2025 challenge," DCASE2025 Challenge, Tech. Rep., 2025.
- [11] B. Han, A. Jiang *et al.*, "Exploring self-supervised audio models for generalized anomalous sound detection," *IEEE Trans. Audio, Speech, Lang. Process.*, pp. 1–15, 2025.
- [12] K. Wilkinghoff, H. Yang *et al.*, "Keeping the balance: Anomaly score calculation for domain generalization," in *Proc. ICASSP*, 2025, pp. 1–5.
- [13] —, "Local density-based anomaly score normalization for domain generalization," *IEEE Trans. Audio, Speech, Lang. Process.*, 2026.
- [14] T. Nishida, N. Harada *et al.*, "Description and discussion on DCASE 2025 challenge task 2: First-shot unsupervised anomalous sound detection for machine condition monitoring," in *Proc. DCASE*, 2025.
- [15] K. Dohi, K. Imoto *et al.*, "Description and Discussion on DCASE 2023 Challenge Task 2: First-Shot Unsupervised Anomalous Sound Detection for Machine Condition Monitoring," in *Proc. DCASE*, 2023.

TABLE VII

VARIANCE-RATIO MEASURES, MEAN-GAP TERMS, AND SENSITIVITY INDEX (d') ACROSS BAND SIZES FOR BAND-PRESERVED FEATURES; ALL METHODS ARE COMPARED WITHOUT LDN.

Dataset	Band size	Var(Sub)/Var(Uni)	Var(Uni)/Var(Glob)	Var(Sub)/Var(Glob)	$\Delta\mu_{\text{Glob}}$	$\Delta\mu_{\text{Sub}}$	d'_{Glob}	d'_{Sub}
BEATs iter3								
DCASE2020	768	0.485	1.023	0.496	0.009	0.008	2.023	2.398
	1536	0.609	1.011	0.616	0.009	0.008	2.023	2.314
	2304	0.686	1.002	0.686	0.009	0.009	2.023	2.258
	3072	0.766	1.006	0.770	0.009	0.009	2.023	2.183
	6144 (global)	1.000	1.000	1.000	0.009	0.009	2.023	2.023
DCASE2023	768	0.538	1.024	0.549	0.007	0.006	0.751	0.851
	1536	0.683	0.998	0.681	0.007	0.006	0.751	0.817
	2304	0.762	0.976	0.741	0.007	0.006	0.751	0.849
	3072	0.822	0.995	0.817	0.007	0.006	0.751	0.793
	6144 (global)	1.000	1.000	1.000	0.007	0.007	0.751	0.751
DCASE2024	768	0.595	1.024	0.612	0.002	0.002	0.450	0.517
	1536	0.720	1.007	0.727	0.002	0.002	0.450	0.506
	2304	0.802	1.032	0.827	0.002	0.002	0.450	0.445
	3072	0.832	0.997	0.830	0.002	0.002	0.450	0.483
	6144 (global)	1.000	1.000	1.000	0.002	0.002	0.450	0.450
Log-Mel								
DCASE2020	12	0.088	1.008	0.085	3.107×10^{-4}	1.134×10^{-4}	1.211	1.199
	25	0.218	1.052	0.219	3.107×10^{-4}	1.798×10^{-4}	1.211	1.281
	38	0.343	1.104	0.368	3.107×10^{-4}	2.186×10^{-4}	1.211	1.298
	51	0.441	1.199	0.520	3.107×10^{-4}	2.417×10^{-4}	1.211	1.241
	128 (global)	1.000	1.000	1.000	3.107×10^{-4}	3.107×10^{-4}	1.211	1.211
DCASE2023	12	0.166	0.632	0.091	7.071×10^{-5}	4.646×10^{-5}	0.116	0.144
	25	0.357	0.748	0.245	7.071×10^{-5}	7.563×10^{-5}	0.116	0.150
	38	0.494	0.884	0.416	7.071×10^{-5}	9.585×10^{-5}	0.116	0.141
	51	0.561	0.954	0.540	7.071×10^{-5}	8.344×10^{-5}	0.116	0.134
	128 (global)	1.000	1.000	1.000	7.071×10^{-5}	7.071×10^{-5}	0.116	0.116
DCASE2024	12	0.124	0.723	0.089	1.177×10^{-4}	2.766×10^{-5}	0.321	0.434
	25	0.352	0.836	0.294	1.177×10^{-4}	4.935×10^{-5}	0.321	0.454
	38	0.465	0.900	0.423	1.177×10^{-4}	7.240×10^{-5}	0.321	0.426
	51	0.594	0.974	0.588	1.177×10^{-4}	7.582×10^{-5}	0.321	0.366
	128 (global)	1.000	1.000	1.000	1.177×10^{-4}	1.177×10^{-4}	0.321	0.321
LPC Spectrum								
DCASE2020	800	0.076	1.959	0.223	0.005	0.002	1.949	2.421
	1600	0.190	2.420	0.455	0.005	0.004	1.949	2.231
	2400	0.284	3.133	0.875	0.005	0.006	1.949	2.775
	3200	0.361	2.716	0.861	0.005	0.006	1.949	3.021
	8000 (global)	1.000	1.000	1.000	0.005	0.005	1.949	1.949
DCASE2023	800	0.124	1.655	0.245	7.735×10^{-4}	6.643×10^{-4}	0.336	0.534
	1600	0.287	1.839	0.595	7.735×10^{-4}	0.001	0.336	0.602
	2400	0.434	2.511	1.242	7.735×10^{-4}	0.002	0.336	0.478
	3200	0.503	2.063	1.101	7.735×10^{-4}	0.002	0.336	0.428
	8000 (global)	1.000	1.000	1.000	7.735×10^{-4}	7.735×10^{-4}	0.336	0.336
DCASE2024	800	0.059	4.184	0.152	2.600×10^{-4}	4.072×10^{-5}	0.177	0.229
	1600	0.169	4.200	0.496	2.600×10^{-4}	1.240×10^{-4}	0.177	0.246
	2400	0.262	3.571	0.888	2.600×10^{-4}	2.118×10^{-4}	0.177	0.251
	3200	0.395	2.687	1.061	2.600×10^{-4}	2.405×10^{-4}	0.177	0.197
	8000 (global)	1.000	1.000	1.000	2.600×10^{-4}	2.600×10^{-4}	0.177	0.177

[16] T. Nishida, N. Harada *et al.*, “Description and discussion on DCASE 2024 challenge task 2: First-shot unsupervised anomalous sound detection for machine condition monitoring,” in *Proc. DCASE*, 2024.

[17] K. Wilkinghoff, “Sub-Cluster AdaCos: Learning Representations for Anomalous Sound Detection,” in *Proc. IJCNN*, 2021, pp. 1–8.

[18] A. Vaswani, N. Shazeer *et al.*, “Attention is all you need,” in *Proc. NeurIPS*, vol. 30, 2017.

[19] S. Chen, Y. Wu *et al.*, “BEATs: Audio pre-training with acoustic tokenizers,” in *Proc. ICML*, 2023.

[20] T. Fujimura, I. Kuroyanagi, and T. Toda, “Improvements of discriminative feature space training for anomalous sound detection in unlabeled conditions,” in *Proc. ICASSP*, 2025, pp. 1–5.

[21] T. Fujimura, K. Wilkinghoff, K. Imoto, and T. Toda, “ASDKit: A toolkit for comprehensive evaluation of anomalous sound detection methods,” *arXiv preprint arXiv:2507.10264*, 2025.

[22] J. P. Burg, “Maximum entropy spectral analysis.” *Ph. D. thesis, Stanford University, Department of Geophysics*, 1975.

[23] N. Andersen, “On the calculation of filter coefficients for maximum entropy spectral analysis,” *Geophysics*, vol. 39, no. 1, pp. 69–72, 1974.

[24] Y. Kawaguchi, K. Imoto *et al.*, “Description and discussion on dcase 2021 challenge task 2: Unsupervised anomalous detection for machine condition monitoring under domain shifted conditions,” in *Proc. DCASE*, Barcelona, Spain, 2021, pp. 186–190.

[25] K. Dohi, K. Imoto *et al.*, “Description and Discussion on DCASE 2022 Challenge Task 2: Unsupervised Anomalous Sound Detection for Machine Condition Monitoring Applying Domain Generalization Techniques,” in *Proc. DCASE*, 2022.

[26] K. Wilkinghoff, T. Fujimura *et al.*, “Handling domain shifts for anomalous sound detection: A review of dcase-related work,” *arXiv preprint arXiv:2503.10435*, 2025.

[27] Y. Koizumi, M. Yasuda *et al.*, “Spidernet: Attention network for one-shot anomaly detection in sounds,” in *Proc. ICASSP*, 2020, pp. 281–285.

[28] T. Hayashi, T. Yoshimura, and Y. Adachi, “Conformer-based id-aware autoencoder for unsupervised anomalous sound detection,” DCASE2020 Challenge, Tech. Rep., Tech. Rep., 2020.

[29] K. Suefusa, T. Nishida *et al.*, “Anomalous Sound Detection Based on Interpolation Deep Neural Network,” in *Proc. ICASSP*, 2020, pp. 271–275.

[30] G. Wichern, A. Chakrabarty, Z.-Q. Wang, and J. L. Roux, “Anomalous Sound Detection Using Attentive Neural Processes,” in *Proc. WASPAA*, 2021, pp. 186–190.

[31] X.-M. Zeng, Y. Song *et al.*, “Joint generative-contrastive representation learning for anomalous sound detection,” in *Proc. ICASSP*, 2023, pp. 1–5.

[32] V. Zavrtnik, M. Marolt, M. Kristan, and D. Skočaj, “Anomalous sound detection by feature-level anomaly simulation,” in *Proc. ICASSP*, 2024, pp. 1466–1470.

[33] N. Harada, D. Niizumi, D. Takeuchi, Y. Ohishi, and M. Yasuda, “First-shot anomaly detection for machine condition monitoring: A domain generalization baseline,” *In arXiv e-prints: 2303.00455*, 2023.

[34] —, “First-shot anomaly detection for machine condition monitoring: A domain generalization baseline,” *Proc. EUSIPCO*, pp. 191–195, 2023.

[35] T. Hayashi, T. Komatsu, R. Kondo, T. Toda, and K. Takeda, “Anomalous

- sound event detection based on wavenet,” in *Proc. EUSIPCO*, 2018, pp. 2494–2498.
- [36] R. Giri, F. Cheng *et al.*, “Group masked autoencoder based density estimator for audio anomaly detection,” in *Proc. DCASE*, 2020.
- [37] W. J. Lee, K. Helwani, A. Krishnaswamy, and S. Tenneti, “Robust audio anomaly detection,” in *RobustML Workshop at ICLR*, May 2021.
- [38] J. Guan, Y. Liu *et al.*, “Time-weighted frequency domain audio representation with gmm estimator for anomalous sound detection,” in *Proc. ICASSP*, 2023, pp. 1–5.
- [39] K. Dohi, T. Endo, H. Purohit, R. Tanabe, and Y. Kawaguchi, “Flow-based self-supervised density estimation for anomalous sound detection,” in *Proc. ICASSP*, 2021, pp. 336–340.
- [40] K. Dohi, T. Endo, and Y. Kawaguchi, “Disentangling physical parameters for anomalous sound detection under domain shifts,” in *Proc. EUSIPCO*, 2021, pp. 279–283.
- [41] D. Hendrycks, M. Mazeika, and T. Dietterich, “Deep anomaly detection with outlier exposure,” *Proc. ICLR*, 2019.
- [42] E. Eskin, A. Arnold, H. Prerau, L. Portnoy, and S. Stolfo, “A Geometric Framework for Unsupervised Anomaly Detection,” in *Applications of Data Mining in Computer Security*. Boston, MA: Springer US, 2002, pp. 77–101.
- [43] R. Giri, S. V. Tenneti *et al.*, “Self-supervised classification for detecting anomalous sounds,” in *Proc. DCASE*, 2020.
- [44] Y. Liu, J. Guan, Q. Zhu, and W. Wang, “Anomalous sound detection using spectral-temporal information fusion,” in *Proc. ICASSP*, 2022, pp. 816–820.
- [45] K. Wilkinghoff, “Self-supervised learning for anomalous sound detection,” in *Proc. ICASSP*, 2024, pp. 276–280.
- [46] Y. Zhang, S. Hongbin, Y. Wan, and M. Li, “Outlier-aware Inlier Modeling and Multi-scale Scoring for Anomalous Sound Detection via Multitask Learning,” in *Proc. Interspeech*. ISCA, 2023, pp. 5381–5385.
- [47] R. Tanaka and S. Tamura, “Few-shot anomalous sound detection based on anomaly map estimation using pseudo abnormal data,” in *Proc. ICASSP*, 2024, pp. 1391–1395.
- [48] K. Wilkinghoff and F. Kurth, “Why Do Angular Margin Losses Work Well for Semi-Supervised Anomalous Sound Detection?” *IEEE/ACM Trans. Audio, Speech, Lang.*, vol. 32, pp. 608–622, 2024.
- [49] Z.-L. Liu, Y. Song, X.-M. Zeng, L.-R. Dai, and I. McLoughlin, “Dp-mae: A dual-path masked autoencoder based self-supervised learning method for anomalous sound detection,” in *Proc. ICASSP*, 2024, pp. 1481–1485.
- [50] K. Wilkinghoff and F. Fritz, “On using pre-trained embeddings for detecting anomalous sounds with limited training data,” in *Proc. EUSIPCO*, 2023, pp. 186–190.
- [51] B. Han, Z. Lv *et al.*, “Exploring large scale pre-trained models for robust machine anomalous sound detection,” in *Proc. ICASSP*, 2024, pp. 1326–1330.
- [52] H. Chen, Y. Song *et al.*, “An effective anomalous sound detection method based on representation learning with simulated anomalies,” in *Proc. ICASSP*, 2023, pp. 1–5.
- [53] X. Zheng, A. Jiang *et al.*, “Improving anomalous sound detection via low-rank adaptation fine-tuning of pre-trained audio models,” in *2024 IEEE Spoken Language Technology Workshop (SLT)*, 2024, pp. 969–974.
- [54] A. Jiang, X. Zheng *et al.*, “Adaptive prototype learning for anomalous sound detection with partially known attributes,” in *Proc. ICASSP*, 2025, pp. 1–5.
- [55] H.-H. Wu, W.-C. Lin *et al.*, “Towards few-shot training-free anomaly sound detection,” in *Proc. Interspeech*, 2025.
- [56] J. F. Gemmeke, D. P. W. Ellis *et al.*, “Audio Set: An ontology and human-labeled dataset for audio events,” in *Proc. ICASSP*, 2017, pp. 776–780.
- [57] A. L. Cramer, H.-H. Wu, J. Salamon, and J. P. Bello, “Look, listen, and learn more: Design choices for deep audio embeddings,” in *Proc. ICASSP*, 2019, pp. 3852–3856.
- [58] Y. Gong, Y.-A. Chung, and J. Glass, “AST: Audio Spectrogram Transformer,” in *Proc. Interspeech 2021*, 2021, pp. 571–575.
- [59] D. Niizumi, D. Takeuchi, Y. Ohishi, N. Harada, and K. Kashino, “Masked spectrogram modeling using masked autoencoders for learning general-purpose audio representation,” in *HEAR: Holistic Evaluation of Audio Representations (NeurIPS 2021 Competition)*, vol. 166, 2022, pp. 1–24.
- [60] H. Dinkel, Y. Wang, Z. Yan, J. Zhang, and Y. Wang, “Ced: Consistent ensemble distillation for audio tagging,” in *Proc. ICASSP*, 2024.
- [61] D. Niizumi, D. Takeuchi, Y. Ohishi, N. Harada, and K. Kashino, “Masked Modeling Duo: Towards a Universal Audio Pre-training Framework,” *IEEE/ACM Trans. Audio, Speech, Lang.*, vol. 32, pp. 2391–2406, 2024.
- [62] D. Niizumi, D. Takeuchi *et al.*, “M2D-CLAP: Masked Modeling Duo Meets CLAP for Learning General-purpose Audio-Language Representation,” *Proc. Interspeech*, 2024.
- [63] W. Chen, Y. Liang, Z. Ma, Z. Zheng, and X. Chen, “Eat: Self-supervised pre-training with efficient audio transformer,” in *Proc. IJCAI*, K. Larson, Ed., 2024, pp. 3807–3815.
- [64] T. Alex, S. Atito, A. Mustafa, M. Awais, and P. J. B. Jackson, “SSLAM: Enhancing self-supervised models with audio mixtures for polyphonic soundscapes,” in *Proc. ICLR*, 2025.
- [65] P. Fan, A. Jiang *et al.*, “Fisher: A foundation model for multi-modal industrial signal comprehensive representation,” *arXiv preprint arXiv:2507.16696*, 2025.
- [66] H. Nam, S.-H. Kim, B.-Y. Ko, and Y.-H. Park, “Frequency Dynamic Convolution: Frequency-Adaptive Pattern Recognition for Sound Event Detection,” in *Proc. Interspeech*, 2022, pp. 2763–2767.
- [67] Y. Guan, G. Zheng, J. Han, and H. Wang, “Subband dependency modeling for sound event detection,” in *Proc. ICASSP*, 2023, pp. 1–5.
- [68] S. Saito and F. Itakura, “Theoretical consideration of the statistical optimum recognition of the spectral density of speech,” *J. Acoust. Soc. Japan*, January 1967.
- [69] J. Makhoul, “Linear prediction: A tutorial review,” *Proceedings of the IEEE*, vol. 63, no. 4, pp. 561–580, 1975.
- [70] L. C. Gleichmann, Y. G. Adhisantoso, A. Lange, and Q. Le Xuan, “Anomaly sound detector based on variational autoencoder with hyper-parameter optimization strategy,” DCASE2024 Challenge, Tech. Rep., 2024.
- [71] T. Nishida, H. Purohit, K. Dohi, T. Endo, and Y. Kawaguchi, “Timbre difference capturing in anomalous sound detection,” in *Proc. EUSIPCO*, 2025.
- [72] L. Bergman, N. Cohen, and Y. Hoshen, “Deep Nearest Neighbor Anomaly Detection,” 2020, arXiv:2002.10445 [cs, stat].
- [73] N. Cohen and Y. Hoshen, “Sub-image anomaly detection with deep pyramid correspondences,” *ArXiv*, vol. abs/2005.02357, 2020.
- [74] K. Roth, L. Pemula *et al.*, “Towards total recall in industrial anomaly detection,” in *Proc. CVPR*, 2022, pp. 14298–14308.
- [75] J. Jeong, Y. Zou *et al.*, “Winclip: Zero-/few-shot anomaly classification and segmentation,” in *Proc. CVPR*, 2023, pp. 19606–19616.
- [76] A. Dosovitskiy, L. Beyer *et al.*, “An image is worth 16x16 words: Transformers for image recognition at scale,” in *Proc. ICLR*, 2021.
- [77] Y. Sha, S. Gou *et al.*, “Regional-local adversarially learned one-class classifier anomalous sound detection in global long-term space,” in *Proc. ACM SIGKDD*, 2022, p. 3858–3868.
- [78] Y. Koizumi, S. Saito, H. Uematsu, N. Harada, and K. Imoto, “ToyAD-MOS: A dataset of miniature-machine operating sounds for anomalous sound detection,” in *Proc. WASPAA*, 2019, pp. 308–312.
- [79] N. Harada, D. Niizumi *et al.*, “ToyADMOS2: Another dataset of miniature-machine operating sounds for anomalous sound detection under domain shift conditions,” in *Proc. DCASE*, 2021, pp. 1–5.
- [80] K. Dohi, T. Nishida *et al.*, “MIMII DG: Sound dataset for malfunctioning industrial machine investigation and inspection for domain generalization task,” in *Proc. DCASE*, Nancy, France, 2022.
- [81] N. Harada, D. Niizumi, Y. Ohishi, D. Takeuchi, and M. Yasuda, “Toy-admos2+: New toyadmos data and benchmark results of the first-shot anomalous sound detection baseline,” DCASE2023 Challenge, Tech. Rep., 2023.
- [82] D. Albertini, F. Augusti, K. Esmer, A. Bernardini, and R. Sannino, “Imad-ds: A dataset for industrial multi-sensor anomaly detection under domain shift conditions,” in *Proc. DCASE*, 2024, pp. 1–5.
- [83] Brian McFee, Colin Raffel *et al.*, “librosa: Audio and Music Signal Analysis in Python,” in *Proc. SciPy*, 2015, pp. 18 – 24.
- [84] J. Deng, J. Guo, N. Xue, and S. Zafeiriou, “Arcface: Additive angular margin loss for deep face recognition,” in *Proc. CVPR*, 2019, pp. 4685–4694.
- [85] I. Loshchilov and F. Hutter, “Decoupled weight decay regularization,” in *Proc. ICLR*, 2017.
- [86] D. S. Park, W. Chan *et al.*, “SpecAugment: A simple data augmentation method for automatic speech recognition,” in *Proc. Interspeech*, 2019.